

## Spectral-weight sum rules for the hadronic vacuum polarization

Diogo Boito<sup>1</sup>, Maarten Golterman<sup>2,3</sup>, Kim Maltman<sup>4,5</sup> and Santiago Peris<sup>3</sup>


<sup>1</sup>*Instituto de Física de São Carlos, Universidade de São Paulo CP 369,  
13570-970, São Carlos, São Paulo, Brazil*

<sup>2</sup>*Department of Physics and Astronomy, San Francisco State University,  
San Francisco, California 94132, USA*

<sup>3</sup>*Department of Physics and IFAE-BIST, Universitat Autònoma de Barcelona  
E-08193 Bellaterra, Barcelona, Spain*

<sup>4</sup>*Department of Mathematics and Statistics, York University Toronto,  
Ontario M3J 1P3, Canada*

<sup>5</sup>*CSSM, University of Adelaide, Adelaide, South Australia 5005 Australia*

 (Received 2 November 2022; accepted 9 February 2023; published 28 February 2023)

We develop a number of sum rules comparing spectral integrals involving judiciously chosen weights to integrals over the corresponding Euclidean two-point function. The applications we have in mind are to the hadronic vacuum polarization that determines the most important hadronic correction  $a_\mu^{\text{HVP}}$  to the muon anomalous magnetic moment. First, we point out how spectral weights may be chosen that emphasize narrow regions in  $\sqrt{s}$ , providing a tool to investigate emerging discrepancies between data-driven and lattice determinations of  $a_\mu^{\text{HVP}}$ . Alternatively, for a narrow region around the  $\rho$  mass, they may allow for a comparison of the dispersive determination of  $a_\mu^{\text{HVP}}$  with lattice determinations zooming in on the region of the well-known *BABAR*-*KLOE* discrepancy. Second, we show how such sum rules can in principle be used for carrying out precision comparisons of hadronic- $\tau$ -decay-based data and  $e^+e^- \rightarrow \text{hadrons}(\gamma)$ -based data, where lattice computations can provide the necessary isospin-breaking corrections.

DOI: 10.1103/PhysRevD.107.034512

### I. INTRODUCTION

As is well known, the recent FNAL E989 experimental result for the muon anomalous magnetic moment  $a_\mu = (g - 2)/2$  [1] confirms the earlier BNL E821 result [2] and produces an updated experimental world average  $4.2\sigma$  larger than the  $g - 2$  theory initiative assessment [3] of the Standard Model (SM) prediction, based on the work of Refs. [4–27]. However, a lattice result for the hadronic vacuum polarization (HVP) contribution  $a_\mu^{\text{HVP}}$  [28] comes out  $2.1\sigma$  higher than the dispersive  $R$ -ratio-based estimate which underlies the SM value of Ref. [3]. Replacing the dispersive estimate for  $a_\mu^{\text{HVP}}$  with the value found in Ref. [28], the SM-based estimate for  $a_\mu$  is only  $1.5\sigma$  lower than the world-average experimental value. As there is no evidence for discrepancies in other contributions to  $a_\mu$ , the recent focus has been on understanding the

discrepancy between the dispersive and lattice values for  $a_\mu^{\text{HVP}}$ .<sup>1</sup>

The dispersive vs lattice discrepancy becomes even more pronounced if we consider the “intermediate window” quantity introduced by RBC/UKQCD [29], in which the integral over Euclidean time,  $t$ , of the lattice correlator that yields  $a_\mu^{\text{HVP}}$  is restricted to a “window” between  $t = 0.4$  and  $t = 1$  fm (smeared by a width of 0.15 fm on both boundaries to avoid lattice artifacts) by multiplying the integrand with a (smoothed-out) double step function in  $t$ . While the original RBC/UKQCD study found agreement between the lattice-based result and the corresponding electro-production-based dispersive estimate, Ref. [30] found a significantly larger lattice value. This larger value was subsequently confirmed in Ref. [28], which produced a lattice result  $3.7\sigma$  above the dispersive estimate. The virtue of the RBC/UKQD intermediate window quantity is that it can be computed with smaller errors on the lattice than the

*Published by the American Physical Society under the terms of the Creative Commons Attribution 4.0 International license. Further distribution of this work must maintain attribution to the author(s) and the published article's title, journal citation, and DOI. Funded by SCOAP<sup>3</sup>.*

<sup>1</sup>For instance, there is good agreement between data-driven and lattice values for the hadronic light-by-light contribution, within  $\lesssim 20\%$  errors. This 20% error corresponds to an uncertainty of about  $2 \times 10^{-10}$  in  $a_\mu$ , which is not sufficient to explain the discrepancy.

quantity  $a_\mu^{\text{HVP}}$  itself, thus allowing more stringent tests between different lattice computations, as well as between lattice and dispersive results.

Meanwhile, the larger lattice values for the intermediate window quantity found in Refs. [28,30] have been confirmed, with different lattice discretizations of the QCD action and the electromagnetic (EM) current, by a number of other groups as well as in updates of the results of Refs. [29,30], in Refs. [31–37].

Clearly, then, it is important to develop further tools to study the discrepancies between dispersive and lattice estimates for  $a_\mu^{\text{HVP}}$  and closely related quantities such as the intermediate window. To obtain dispersive estimates for the window quantity, which is defined as a function of Euclidean time, the window function needs to be converted to a window in  $\sqrt{s}$ , the center-of-mass energy in  $e^+e^- \rightarrow$  hadrons. As a function of  $\sqrt{s}$ , however, the weight which defines the intermediate window is very broad, ranging from about 0.7 GeV to 3 GeV (taking the values of  $\sqrt{s}$  where it exceeds roughly half of its maximum value). To explore the lattice vs dispersive discrepancy in more detail, it would be useful to have access to tools to compare data-driven dispersive results with lattice results in narrower, more “custom-designed” windows in  $\sqrt{s}$ . In this paper, we propose a class of sum rules designed with precisely this goal in mind. Similar ideas were recently explored in Ref. [38], by considering linear combinations of a set of Euclidean windows, and in Ref. [39]. Here, instead, we define the weights we will employ in our weighted spectral integrals directly as a function of  $s$ , and derive sum rules relating these weighted spectral integrals to integrals in Euclidean time over correlation functions which can be evaluated on the lattice.

In Sec. II we develop two sets of sum rules starting from weights defined as a function of  $s$ . In Sec. II A we consider a class of rational weights that allow us to define windows localized in  $s$ . They are similar to those used recently in Ref. [40] to obtain a lattice-based determination of  $|V_{us}|$  from strange hadronic  $\tau$ -decay data. In Sec. II B we use these rational weights as the starting point for defining a set of sum-of-exponential weights with shapes very similar to those defined by the underlying rational weights, following ideas proposed in Ref. [41]. In both cases exact sum rules exist relating spectral integrals employing these weights to quantities that can be directly computed on the lattice. We explain why the sum-of-exponential weights may lead to smaller errors for the lattice side of the sum rules than the corresponding rational weights, and provide examples of this reduction in Sec. III.

Narrower windows in  $\sqrt{s}$  are also potentially useful for comparing  $I = 1$  contributions to  $a_\mu^{\text{HVP}}$  inferred from  $I = 1$  hadronic  $\tau$ -decay data with the corresponding contributions obtained using  $R$ -ratio data. An example of the potential usefulness of narrower windows is the application to the BABAR-KLOE discrepancy in the two-pion spectral

distributions (for a review, see Ref. [3]), where the discrepancy occurs over a fairly narrow range in energy around the  $\rho$  peak. Attempts to use  $\tau$ -based data have a long history [42–45], but have been abandoned more recently because of the increased precision of electroproduction data and the lack of a solid theoretical framework for evaluating the isospin-breaking (IB) corrections that must be applied to the  $\tau$ -based data. It would be interesting to revisit this possibility since (i) a more precise  $\tau$ -based nonstrange vector spectral function is now available [46], and (ii) Belle II may provide improved  $\tau$ -decay-distribution data for at least some of the most important vector-channel exclusive modes [47,48]. Moreover, we will argue in Sec. IV of this paper that if the combined  $2\pi$  and  $4\pi$  channels are taken from  $\tau$ , then, to good accuracy, the lattice can be used to compute the necessary IB corrections from first principles. We illustrate the comparison of electroproduction- and hadronic- $\tau$ -decay-based  $2\pi + 4\pi$  data using two rational weight choices,  $W_{1,5}$  and  $W_{2,5}$ , defined in Sec. III.

We end the paper with a brief conclusion in Sec. V, and relegate some technical details to two appendices.

## II. SUM RULES

In this section, we develop two types of sum rules, one, in Sec. II A, based on a set of weights used before in Ref. [40], and one, in Sec. II B, based on the ideas advocated in Ref. [41]. They are closely related, and we will explore their differences in examples in Sec. III.

We start from a Euclidean current-current correlator

$$G_{\mu\nu}(x) = \langle j_\mu(0)j'_\nu(x) \rangle = \int \frac{d^4q}{(2\pi)^4} e^{iqx} (\delta_{\mu\nu}q^2 - q_\mu q_\nu) \Pi(q^2) \quad (2.1)$$

for two potentially different vector currents  $j_\mu$  and  $j'_\nu$ , and define from this the time-momentum correlator  $C(t)$  by

$$\begin{aligned} C(t) &= -\frac{1}{3} \sum_{k=1}^3 \int d^3x \langle j_k(0)j'_k(\vec{x}, t) \rangle \\ &= -\int \frac{dQ}{2\pi} e^{iQ_t} Q^2 \Pi(Q^2), \end{aligned} \quad (2.2)$$

where  $Q = q_4$ , and we have assumed that a regulator (such as the lattice) has been introduced, so that  $C(t)$  and  $\Pi(Q^2)$  are finite. While in straightforward applications to  $a_\mu^{\text{HVP}}$  the currents  $j_\mu$  and  $j'_\nu$  will both be the hadronic electromagnetic current, they can also be chosen different, as will be done in the application described in Sec. IV below. The corresponding subtracted polarization

$$\hat{\Pi}(Q^2) = \Pi(Q^2) - \Pi(0) \quad (2.3)$$

can be expressed in terms of  $C(t)$  by

$$\begin{aligned}
\hat{\Pi}(Q^2) &= -\frac{1}{Q^2} \int_{-\infty}^{\infty} dt (e^{iQt} - 1) C(t) - \Pi(0), \\
&= -\frac{2}{Q^2} \int_0^{\infty} dt (\cos(Qt) - 1) C(t) - \Pi(0), \\
&= \int_0^{\infty} dt \left( \frac{4 \sin^2(Qt/2)}{Q^2} - t^2 \right) C(t), \quad (2.4)
\end{aligned}$$

where we used  $\int dt C(t) = 0$  and, in the second step, that  $C(t)$  is an even function of  $t$ . We define the spectral function  $\rho(s)$  as usual by

$$\rho(s) = \frac{1}{\pi} \text{Im} \Pi(s), \quad (2.5)$$

with  $\hat{\Pi}(Q^2)$  and  $\rho(s)$  satisfying the subtracted dispersion relation

$$\hat{\Pi}(Q^2) = -Q^2 \int_{s_{\text{th}}}^{\infty} ds \frac{\rho(s)}{s(s+Q^2)}, \quad (2.6)$$

with  $s_{\text{th}}$  the relevant threshold value for  $\rho(s)$ .

### A. Rational-weight sum rules

We begin with a set of spectral weights of the form

$$\begin{aligned}
W_{m,n}(s; \{Q_\ell^2\}) &= \mu^{2(n-m-1)} \frac{(s - s_{\text{th}})^m}{\prod_{\ell=1}^n (s + Q_\ell^2)}, \\
Q_n^2 &> Q_{n-1}^2 > \dots > Q_1^2 > 0. \quad (2.7)
\end{aligned}$$

Here the  $Q_\ell^2$  are a set of fixed Euclidean squared momenta, and we will always take  $m$  sufficiently smaller than  $n$  that the weighted spectral integral with weight (2.7) is finite. We multiply by a generic mass scale  $\mu^{2(n-m-1)}$  to make the weighted spectral integrals considered below dimensionless; any precisely known scale is suitable for this purpose and we will employ the choice  $\mu = m_\tau$  in what follows.

We then consider the integral

$$\begin{aligned}
&\frac{1}{2\pi i} \int_C dz W_{m,n}(z; \{Q_\ell^2\}) \Pi(-z) \\
&= (-1)^m m_\tau^{2(n-m-1)} \sum_{k=1}^n \frac{(Q_k^2 + s_{\text{th}})^m}{\prod_{\ell \neq k} (Q_\ell^2 - Q_k^2)} \Pi(Q_k^2), \quad (2.8)
\end{aligned}$$

with  $C$  as the contour in the complex  $z = q^2 = -Q^2$  plane shown in Fig. 1, assumed to have a radius large enough that all the  $z = -Q_k^2$  points lie in its interior on the negative  $z$  axis. The result on the right-hand side follows from the fact that  $\Pi(-z)$  is analytic in the complex plane except for a cut starting at  $s_{\text{th}}$  on the positive real  $z$  axis, as shown in Fig. 1. If we now take the radius of the circular part of  $C$  to infinity, we obtain the sum rule

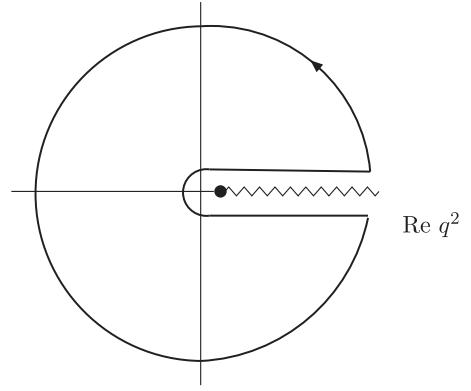


FIG. 1. Contour  $C$  used in Eq. (2.8):  $z = q^2 = -Q^2$ . The black dot indicates the point  $q^2 = s_{\text{th}}$ .

$$\begin{aligned}
I_{m,n} &\equiv \int_{s_{\text{th}}}^{\infty} ds W_{m,n}(s; \{Q_\ell^2\}) \rho(s) \\
&= (-1)^m m_\tau^{2(n-m-1)} \sum_{k=1}^n \frac{(Q_k^2 + s_{\text{th}})^m}{\prod_{\ell \neq k} (Q_\ell^2 - Q_k^2)} \Pi(Q_k^2), \quad (2.9)
\end{aligned}$$

where the integral over the spectral function comes from the discontinuity along the positive real  $z$  axis. We will prove in Appendix A that

$$\sum_{k=1}^n \frac{(Q_k^2 + s_{\text{th}})^m}{\prod_{\ell \neq k} (Q_\ell^2 - Q_k^2)} = 0, \quad (2.10)$$

from which it follows that we can replace  $\Pi(Q_k^2)$  by  $\hat{\Pi}(Q_k^2)$  on the right-hand side of Eq. (2.9). This has to be the case, as the left-hand side is finite by construction, and thus the term proportional to  $\Pi(0)$  on the right-hand side has to vanish.

A potentially useful application of this sum rule is to evaluate the spectral integral using data, for instance obtained from  $R$ -ratio measurements, and the sum on the right-hand side using data from lattice QCD. In fact, what is usually computed in lattice QCD is a position-space correlator; in the case of  $a_\mu^{\text{HVP}}$ , Eq. (2.2) with  $j_\mu = j'_\mu$  the hadronic electromagnetic current. Replacing  $\Pi(Q_k^2)$  with  $\hat{\Pi}(Q_k^2)$  and using Eq. (2.4), the sum rule (2.9) can then be recast as

$$\int_{s_{\text{th}}}^{\infty} ds W_{m,n}(s; \{Q_\ell^2\}) \rho(s) = \int_0^{\infty} dt c^{(m,n)}(t) C(t), \quad (2.11)$$

with

$$\begin{aligned}
c^{(m,n)}(t) &= (-1)^m m_\tau^{2(n-m-1)} \sum_{k=1}^n \frac{(Q_k^2 + s_{\text{th}})^m}{\prod_{\ell \neq k} (Q_\ell^2 - Q_k^2)} \\
&\times \left( \frac{4 \sin^2(Q_k t/2)}{Q_k^2} - t^2 \right). \quad (2.12)
\end{aligned}$$

We will refer to the sum rules of Eq. (2.11) as “rational-weight sum rules” (RWSRs). On the lattice, the integral over  $t$  on the right-hand side of Eq. (2.11) would be replaced by a sum over the discrete values of  $t$  available on the lattice, using, for example, the trapezoidal rule. We will discuss examples in Sec. III A below.

### B. Exponential-weight sum rules

The sum rules of Eq. (2.11) require the evaluation of  $C(t)$  at all values of  $t$ . In lattice QCD, the signal-to-noise ratio for  $C(t)$  deteriorates when  $t$  gets large, and the contributions for these larger  $t$  values will thus “degrade” the precision with which the right-hand side of Eq. (2.11) can be computed.

In this section, we therefore develop modified sum rules, involving new weights constructed to require the evaluation of  $C(t)$  at only a limited set of  $t$  values. While these new weights will, of necessity, differ from the old weights  $W_{m,n}$ , we will see that, following the ideas of Ref. [41], it is possible to choose them to be remarkably similar to the  $W_{m,n}$ .

We begin with the observation that

$$C(t) = \int_{E_{\text{th}}}^{\infty} dE \rho(E^2) (E^2 e^{-E|t|} - 2E\delta(t)), \quad (2.13)$$

with  $E_{\text{th}} = \sqrt{s_{\text{th}}}$  the threshold energy. The term proportional to  $\delta(t)$  ensures that  $\int dt C(t) = 0$ .<sup>2</sup> We then define new weights

$$w_n(E; \{t_j\}, \{x_j\}) = \sum_{j=1}^n x_j (E^2 e^{-|t_j|E} - 2E\delta(t_j)), \quad (2.14)$$

with  $\{t_j\}$  a fixed set of  $t$  values and  $\{x_j\}$  a set of coefficients to be determined below. In all our applications, the  $t_j$  will be chosen positive, and we can ignore the term with the  $\delta$  function. The  $w_n(E; \{t_j\}, \{x_j\})$ -weighted spectral integrals then satisfy sum rules,

$$\int_{E_{\text{th}}}^{\infty} dE \rho(E^2) w_n(E; \{t_j\}, \{x_j\}) = \sum_{j=1}^n x_j C(t_j), \quad (2.15)$$

in which only the  $n$  values  $C(t_j)$  occur on the right-hand side.

The goal then is to start with an initial weight,  $W(s)$ , having some desired  $s$  dependence [for example, one of the weights  $W_{m,n}(s, \{Q_\ell^2\})$ ] and find a set of  $n$ ,  $\{t_j\}$  and  $\{x_j\}$  such that the associated  $w_n(E; \{t_j\}, \{x_j\})$  represents a close approximation to the weight  $2EW(s = E^2)$  appearing in the alternate,  $E$ -dependent expression

$$\int_{s_{\text{th}}}^{\infty} ds W(s) \rho(s) = \int_{E_{\text{th}}}^{\infty} dE 2EW(E^2) \rho(E^2) \quad (2.16)$$

for the  $W(s)$ -weighted spectral integral. If such a choice exists, the associated sum rule, Eq. (2.15), will involve a spectral integral whose weighting, by construction, is similar to that of the desired original  $W(s)$ -weighted spectral integral, but whose right-hand side involves values of  $C(t)$  at only the finite number of chosen  $t$ .

The key point is that it is indeed possible, using the method of Ref. [41], to choose  $n$ , the  $\{t_j\}$  and the  $\{x_j\}$  such that  $w_n(E; \{t_j\}, \{x_j\})$  provides a very good approximation to  $2EW(s = E^2)$  for weight choices, like  $W(s) = W_{m,n}(s, \{Q_\ell^2\})$ , of interest in exploring the  $a_\mu^{\text{HVP}}$  problem. While in what follows we focus, to be specific, on examples with  $W(s) = W_{m,n}(s = E^2; \{Q_\ell^2\})$ , we stress that the method is applicable to more general initial weight choices as well.

The construction of Ref. [41] proceeds as follows. Starting with an initial desired weight  $W(s)$ , to be referred to in what follows as the “pre mold,” we choose a set of (positive)  $t$  values  $\{t_j\}$ ,  $j = 1, \dots, n$ , and minimize

$$\int_{E_{\text{th}}}^{\infty} \frac{dE}{E^4} |w_n(E; \{t_j\}, \{x_j\}) - 2EW(E^2)|^2 \quad (2.17)$$

with respect to the parameters  $x_j$ ,  $j = 1, \dots, n$ . We denote the parameter values which accomplish this minimization by  $\{x_j^W\}$ . The result is a  $w_n(E; \{t_j\}, \{x_j^W\})$  which represents a (close) approximation to  $2EW(E^2)$ , one having the form of  $E^2$  times a weighted sum of exponentials. We will refer to the product  $2EW(E^2)$  as the “mold,” and the approximation  $w_n(E; \{t_j\}, \{x_j^W\})$  as the “cast.” The sum rule Eq. (2.15) then takes the form

$$I_{W'} \equiv \int_{E_{\text{th}}}^{\infty} dE \rho(E^2) w_n(E; \{t_j\}, \{x_j^W\}) = \sum_{j=1}^n x_j^W C(t_j), \quad (2.18)$$

where the subscript/superscript  $W$  emphasizes the role of the underlying pre mold function,  $W(s)$ , while the prime reminds us that the spectral integral is evaluated with the derived cast  $w_n$ . We will refer to sum rules of the form (2.18) as “exponential-weight sum rules” (EWSRs). Equation (2.17) is solved by

$$x_i = \sum_{j=1}^n A_{ij}^{-1} f_j, \quad (2.19)$$

with the matrix  $A$  and the input vector  $f$  defined by

<sup>2</sup>This term is formally divergent, but, as before, we assume that  $C(t)$  has been regulated.

$$A_{ij} = \int_{E_{\text{th}}}^{\infty} dE e^{-(t_i+t_j)E}, \quad f_i = 2 \int_{E_{\text{th}}}^{\infty} dE e^{-t_i E} W(E^2)/E. \quad (2.20)$$

At this point, we depart from the philosophy of Ref. [41]: we throw away the mold and keep the cast. If the cast is a good approximation of the mold, it will serve equally well for comparing experimental data, represented by  $\rho(s)$ , with lattice data, represented by  $C(t)$ , in the region of energies characterized by the mold, and there is thus no need to keep the mold. Instead, we work directly with the cast sum rule, Eq. (2.18).

Following this philosophy, there is also no need to keep the values of the  $x_j$  obtained from Eq. (2.19) to a very high precision. One can keep a fixed number of digits, and declare the values chopped off after the last of these digits as the exact values of the  $x_j$  to be used. The only requirement is that the thus-defined exponential weight still fulfills the goal for which it was designed, i.e., that it probes the desired energy range. In our examples in the next section, we will chop off the  $x_j$  values at six digits, *cf.* Eqs. (3.5) and (3.6).

The only role of the premold and mold functions in this approach is to fix the type of weighting one wants in the weighted spectral integral in cases (such as exploring the BABAR-KLOE discrepancy) where the desired weighting is naturally formulated in the  $s$ -space spectral integral representation. The cast then provides a similarly weighted spectral integral having the advantage that the corresponding weighted Euclidean integral is trivially written down using the exact sum rule (2.18) above. Attempting to find a set of  $x_j$  which produces such a desired spectral integral weighting is a much more challenging task without the intermediate step of first setting up the mold function and using it to find a set of  $x_j$  which implement the Euclidean representation corresponding to the closely related  $s$ -dependent cast weighting. We will discuss examples of this strategy in Sec. III B, where the premolds will be the weights we consider in Sec. III A.

It is important to realize that, once one has a cast, i.e., one has chosen the set  $\{t_j\}$  and a strategy for determining the associated coefficients  $\{x_j\}$ , the resulting sum rule, (2.18), is *exact*. Different choices for the set  $\{t_j\}$  produce different cast functions, even when starting from the same pre-mold. These different casts, moreover, all differ from their original pre-mold(s). The exact cast sum rules corresponding to different cast choices are then just that, different exact sum rules in their own right, and not to be thought of as approximations to the (equally exact) premold sum rule. Differences in the values of the left-hand sides (or right-hand sides) of the sum rules (2.18) corresponding to different cast choices thus simply reflect the fact that those sum rules involve different weights. Such differences in no

way constitute an additional systematic uncertainty on the values of any of the individual cast sum rules.<sup>3</sup>

To illustrate the freedom to choose different casts, we discuss one more variant. For the types of weight functions we consider in this paper, the matrix  $A$  defined in Eq. (2.20) may have very small eigenvalues, and, correspondingly, the  $x_j^W$  values may span a rather large range [as in Eqs. (3.5) and (3.6) below], leading to potentially sizeable cancellations and possible error inflation. We may reduce this range by modifying the matrix  $A$  to some extent, while keeping the cast close to the mold, so that the modified sum rule still probes essentially the same range in  $\sqrt{s}$ . The specific modification we will consider is to replace the matrix  $A$  with the related matrix  $\hat{A}$ , defined by

$$\hat{A}(\lambda) = (1 - \lambda)A + \lambda \mathbf{1}_n, \quad (2.21)$$

where  $\mathbf{1}_n$  is the  $n \times n$  unit matrix. This simply replaces eigenvalues of  $A$  much smaller than  $\lambda$  with new eigenvalues of order  $\lambda$ , leaving eigenvalues much larger than  $\lambda$  essentially unchanged. We thus expect, and indeed find to be the case below, that if we choose  $\lambda$  larger than the smallest eigenvalue of  $A$  the range of the  $x_j^W$  values, and hence the error on the lattice sides of the resulting EWSRs, will be reduced. We will denote the analog of the spectral integral  $I_W$  of Eq. (2.18) obtained using the modified set of  $x_j^W$  resulting from this replacement by  $I_{\hat{W}}$  in what follows.

We close this subsection with a recap of the key points of the motivation for the EWSR construction. The goal of this paper is to provide a method for exploring the tension between lattice and dispersive results for  $a_\mu^{\text{HVP}}$  by identifying  $s$ -dependent weights,  $W(s)$ , which are simultaneously localized to relatively narrow regions in  $s$  and such that the alternate, Euclidean-time ( $t$ ) representations of the  $W(s)$ -weighted spectral integrals,  $I_W$ , evaluated using input lattice data, have errors small enough to make the resulting dispersive-lattice comparison numerically interesting. Such dispersive-lattice comparisons are, in principle, possible for any  $W(s)$ , provided both the spectral data and lattice data are known to sufficiently high precision. In practice, however, lattice errors grow rapidly at large Euclidean  $t$ . The  $I_W$  produced by the vast majority of  $W(s)$  have, as in the case of the RWSR examples above, equivalent

<sup>3</sup>This remark should be kept in mind when considering the results in Sec. III B below. The results quoted in the first (or second) lines of Eqs. (3.12) and (3.13), for example, correspond to the same premold choice, but different choices of the related cast. The (slightly different) cast choices produce (slightly different) central values for the (weight-dependent) right-hand sides of the corresponding cast sum rules. These values, of course, also differ slightly from those of the right-hand sides of the sum rules corresponding to the (also slightly different) premold weights, given in Eq. (3.3). The results of Eqs. (3.3), (3.12), and (3.13) are those of three independent sum rules involving three different weights.

Euclidean- $t$  representations which contain contributions from  $C(t)$  at arbitrarily large  $t$ , and hence typically have enhanced errors when evaluated using real-world lattice data. The EWSR construction, in restricting by hand the range of Euclidean  $t$  for which lattice results for  $C(t)$  are required, allows one to mitigate this problem, while at the same time retaining the desired qualitative  $s$ -dependent weighting.

Another way of describing what is going on in the EWSR construction is as follows: given a typical premold,  $W(s)$ , chosen with a particular localization in  $s$  in mind, the Euclidean- $t$  representations equivalent to the spectral integrals produced by, not just that premold, but also the vast majority of qualitatively similar “nearby” weights, will all suffer from the error-enhancing feature of having nontrivial support at large Euclidean  $t$ . The EWSR construction, however, shows that this is not a generic feature of all such “nearby” weights: weights  $V(s)$  qualitatively similar to  $W(s)$  exist for which the corresponding weighted spectral integral has a Euclidean- $t$  representation with no support whatsoever beyond the maximum  $t$  employed in constructing  $V(s)$ . We expect such special “nearby” weights to produce equivalent lattice evaluations of  $I_V$  with significantly reduced relative errors, and show, in Sec. III B, that this expectation is, indeed, borne out. An important lesson to be drawn from this observation is that, when real-world lattice errors are taken into account,  $s$ -dependent weights which are very similar as functions of  $s$  may differ significantly in how accurately the equivalent lattice representations of their weighted spectral integrals can be evaluated. Sum rules based on judicious choices of EWSR weights,  $V(s)$ , constructed starting from generic premolds,  $W(s)$ , are thus likely to represent better choices for use in exploring dispersive-lattice differences than would the apparently rather similar sum rules based on the underlying generic premolds.

### III. EXAMPLE: APPLICATION TO COMPARISON BETWEEN EXPERIMENTAL AND LATTICE DATA

We will now turn to two numerical examples, using two different weights  $W_{m,n}$  of the type (2.7), both with  $s_{\text{th}} = 4m_\pi^2$  and

$$Q_\ell^2 = 0.25 + 0.075(\ell - 1) \text{ GeV}^2, \quad \ell = 1, \dots, 5. \quad (3.1)$$

The first has  $m = 1$ ,  $n = 5$ , and the second  $m = 2$ ,  $n = 5$ . We choose  $m_\pi = 134.977$  MeV and  $m_\tau = 1776.86$  MeV. These two weights are plotted as a function of  $\sqrt{s}$  in Fig. 2, where  $W_{2,5}$  has been multiplied by a factor of 15 to show it on approximately the same scale as  $W_{1,5}$ .<sup>4</sup> The weight  $W_{2,5}$

<sup>4</sup>The absolute scale of the weights is arbitrary, as long as the same scale is used on both sides of the sum rules.

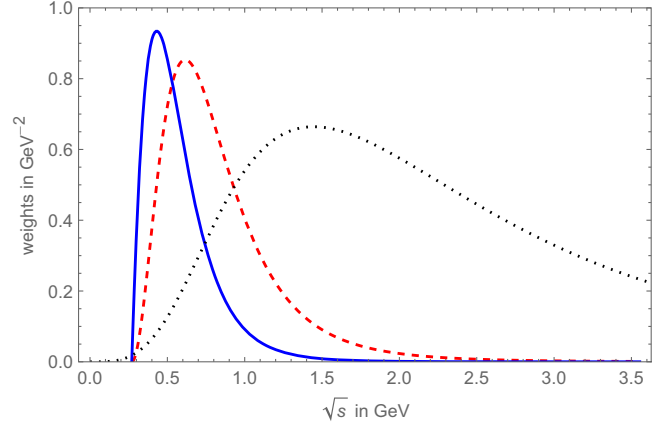


FIG. 2. The weights  $W_{1,5}$  (blue, solid), and  $15 \times W_{2,5}$  (red, dashed) with  $Q_\ell^2$  defined in Eq. (3.1). ( $W_{2,5}$  is multiplied by a factor of 15 for clarity.) The black dotted curve shows the “intermediate window” weight of Ref. [29], transformed to the equivalent  $\sqrt{s}$ -dependent form [38].

overlaps better with the region dominated by the  $\rho$ , but falls off more slowly for large  $s$ . The value of  $n - m$  is smaller for  $W_{2,5}$  than for  $W_{1,5}$ , which leads us to expect a smaller error on the right-hand side of the  $W_{2,5}$  sum rule, according to Appendix A. For comparison, we also show the Minkowski version [38] of the “intermediate window” weight introduced as a function of  $t$  in Ref. [29]. These weights will be used for a study of the sum rule (2.11) in Sec. III A and a study of the sum rule (2.18) in Sec. III B.

In Fig. 3 we show the functions  $c^{(1,5)}(t)$  and  $c^{(2,5)}(t)$  defined in Eq. (2.12), multiplied by  $10^{-5}$  and  $15 \times 10^{-5}$ , respectively. We see that these functions have the bulk of their support toward larger  $t$ , while being very small at values of  $t$  smaller than approximately 1 fm. This is not surprising, as the weights  $W_{1,5}(s)$  and  $W_{2,5}(s)$  have their support at relatively small  $\sqrt{s}$ . We will see below to what extent this has an effect on the size of the errors with which the right-hand side of Eq. (2.11) can be evaluated.

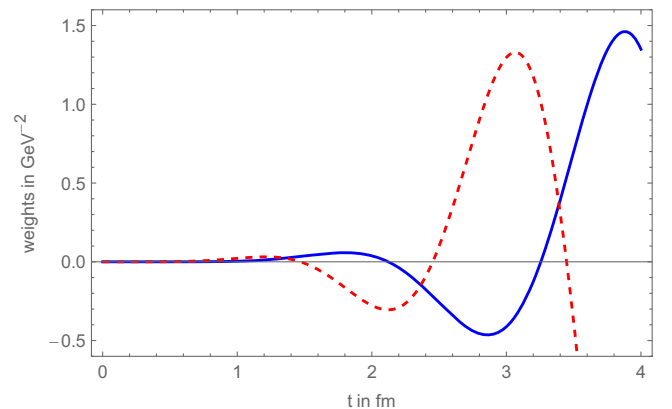


FIG. 3. The weights  $10^{-5}c^{(1,5)}(t)$  (blue) and  $15 \times 10^{-5}c^{(2,5)}(t)$  (red) with  $Q_\ell^2$  as in Eq. (3.1).

TABLE I. The right-hand sides of Eq. (2.11) for the lattice ensembles of Ref. [33]. The columns to the left of the double vertical line contain the label of the ensemble, the lattice spacing  $a$ , the spatial/temporal extent,  $L^3 \times T$  (in lattice units), and the Nambu-Goldstone pion mass  $m_\pi$ . The columns to the right of the double line contain the integrals  $I_{W_{1.5}}(\text{rhs})$  and  $I_{W_{2.5}}(\text{rhs})$ .

Label	$a$ (fm)	$L^3 \times T$	$m_\pi$ (MeV)	$I_{W_{1.5}}(\text{rhs})$	$I_{W_{2.5}}(\text{rhs})$
96	0.05684	$96^3 \times 192$	134.3	0.463(45)	0.0860(74)
64	0.08787	$64^3 \times 96$	129.5	0.453(23)	0.0826(28)
48I	0.12121	$48^3 \times 64$	132.7	0.426(13)	0.0831(13)
32	0.15148	$32^3 \times 48$	133.0	0.433(13)	0.0801(17)
48II	0.15099	$48^3 \times 64$	134.3	0.411(14)	0.0824(18)

In these examples, we will use the combined  $R$ -ratio data from Ref. [11] to evaluate the weighted spectral integrals on the left-hand side (lhs) and the light-quark-connected lattice data from Ref. [33] to evaluate the weighted integrals over  $C(t)$  on the right-hand side (rhs).<sup>5</sup> Since the data from Ref. [33] are for the light-quark-connected part only, this is a comparison between apples and oranges as far as the central results are concerned. Here, however, we are interested in seeing the size of typical errors on each side of the sum rule, and using these immediately accessible recent data sources suffices for this purpose. We emphasize that our intent is to investigate the size of lattice and spectral integral errors in our proposed methodology, and that, at present, no conclusions should be drawn from the level of numerical agreement between the two sides of the sum rules considered throughout Sec. III. We also neglect corrections to the lattice data of Ref. [33] for finite-volume, taste-breaking and pion-mass mistuning effects, having convinced ourselves that these corrections are small, and do not lead to qualitative changes in the conclusions we obtain below. This is consistent with our intent to study the methodology of these sum rules, leaving concrete applications to the future.

### A. Examples using rational-weight sum rules

We begin with the values of the spectral integrals appearing on the lhs of the sum rule (2.11) for the weights  $W_{1.5}$  and  $W_{2.5}$  obtained using the  $R$ -ratio data from Ref. [11]. We find

$$\begin{aligned} I_{W_{1.5}}(\text{lhs}) &= 0.4756(16), \\ I_{W_{2.5}}(\text{lhs}) &= 0.09107(34). \end{aligned} \quad (3.2)$$

Both spectral integrals are obtained with a precision better than 0.4%.

We next turn to the evaluation of the rhss of the  $W_{1.5}$  and  $W_{2.5}$  RWSRs using lattice data for the light-quark connected contribution to the correlator  $C(t)$  obtained using

<sup>5</sup>The results of Ref. [33] were obtained using ensembles from Refs. [49,50].

the five ensembles of Ref. [33]. Table I shows the ensemble parameters to the left of the double vertical line, and the associated finite-lattice-spacing results for  $I_{W_{1.5}}(\text{rhs})$  and  $I_{W_{2.5}}(\text{rhs})$  to the right of it. We note that the values of the pion mass and the volume differ from ensemble to ensemble, and would, in principle, need to be adjusted to common values before carrying out an extrapolation to the continuum limit. Since, however, the current statistical errors are large enough that these mistunings would make no difference in practice, we have, instead, neglected such corrections, and carried out an extrapolation linear in  $a^2$  to the continuum limit. For the  $a = 0.15$  fm lattice spacing we chose the larger of the two volumes, not using the 32 ensemble. The fits have excellent  $p$ -values, and we find the continuum-limit values

$$\begin{aligned} I_{W_{1.5}}(\text{rhs}) &= 0.468(26), \\ I_{W_{2.5}}(\text{rhs}) &= 0.0838(33). \end{aligned} \quad (3.3)$$

These integrals have a precision of 5.6%, respectively, 3.9%.<sup>6</sup> Based on these results we make the following observations. First, the errors in Eq. (3.3) are large, and a significant reduction in errors would be needed to make these sum rules useful. However, as we will see in the next subsection, errors on the rhs, obtained using the same lattice data, are smaller for sum rules of the type (2.18) than for those of the type (2.11). Second, from the different size of the errors for the sum rules with  $W_{1.5}$  and  $W_{2.5}$ , it is clear that a fine-tuning of the rational weight may be necessary to make optimal use of a certain set of lattice data. We emphasize again that the numbers in Eqs. (3.2) and (3.3) should not be directly compared in this example, because, in this pilot study, we used the fully inclusive data on the lhs, but only light-quark-connected data on the rhs. Of course, fully inclusive lattice data are becoming available, and with such data, a direct comparison will be possible. It is, moreover, reasonable to expect such lattice data to have significantly improved errors, allowing for significant improvements to the relative errors in Eq. (3.3) as well.

### B. Examples using exponential-weight sum rules

We now turn to sum rules of the type (2.18), using as examples of the pre-mold the weights  $W_{1.5}$  and  $W_{2.5}$  of Sec. III A. We still need to choose the  $t_j$  appearing in Eq. (2.18) and, in this section, will employ the following values, given in units of  $\text{GeV}^{-1}$ :

$$t_1 = 3, \quad t_2 = 6, \quad t_3 = 9, \quad t_4 = 12, \quad t_5 = 15. \quad (3.4)$$

<sup>6</sup>The relatively large errors make the figures showing these fits not very interesting, and we thus omit them. In the next subsection we will show the equivalent fits for the EWSRs, for which the lattice values have smaller errors.

Since these values do not exactly coincide with the values of  $t$  available for the lattice ensembles we employ, we obtain the associated  $C(t_j)$  values, in all cases, by linear interpolation from the nearest available  $t$ , taking into account all correlations in the interpolation. The range of values in Eq. (3.4) is one for which lattice computations of  $C(t)$  generally have small statistical errors.

With the  $t_j$  defined, the values of the coefficients  $x_j$  are fixed by the premold choice. For  $W'_{1,5}$  we find

$$W'_{1,5}: x_1 = 37.4123, \quad x_2 = 2625.13, \quad x_3 = 25912.1, \\ x_4 = -106707, \quad x_5 = 78192.8, \quad (3.5)$$

while for  $W'_{2,5}$  we find

$$W'_{2,5}: x_1 = 34.0249, \quad x_2 = 870.640, \quad x_3 = -5501.14, \\ x_4 = 9933.01, \quad x_5 = -5284.24. \quad (3.6)$$

For  $\hat{W}_{1,5}$  and  $\hat{W}_{2,5}$ , obtained by replacing  $A$  by the  $\lambda = 10^{-9}$  version of  $\hat{A}$  of Eq. (2.21) in Eq. (2.19), we find

$$\hat{W}_{1,5}: x_1 = -78.8487, \quad x_2 = 5688.30, \quad x_3 = 2223.96, \\ x_4 = -36638.0, \quad x_5 = 8047.38, \quad (3.7)$$

and

$$\hat{W}_{2,5}: x_1 = 44.8916, \quad x_2 = 590.933, \quad x_3 = -3373.53, \\ x_4 = 3716.86, \quad x_5 = 879.149. \quad (3.8)$$

As already explained in Sec. II B, we will use these exact values in the rest of this subsection.

In the upper panels of Fig. 4 we show the molds  $2\sqrt{s}W_{1,5}(s)$  and  $2\sqrt{s}W_{2,5}(s)$  together with their associated casts,  $W'_{1,5}(s) = w_5(E; \{t_j\}, \{x_j^{W'_{1,5}}\})$  and  $W'_{2,5}(s) = w_5(E; \{t_j\}, \{x_j^{W'_{2,5}}\})$ , determined by Eqs. (3.4)–(3.6). We also show the casts  $\hat{W}_{1,5}(s) = w_5(E; \{t_j\}, \{x_j^{\hat{W}_{1,5}}\})$  and  $\hat{W}_{2,5}(s) = w_5(E; \{t_j\}, \{x_j^{\hat{W}_{2,5}}\})$ , determined with Eqs. (3.7) and (3.8) instead. On the scale of these figures, the casts are almost indistinguishable from the underlying molds for the  $A$ -based casts, and quite close for the  $\hat{A}$ -based casts. The smaller-vertical-scale lower panels show the corresponding cast-mold differences in more visually evident form.

As for the RWSR cases, we first give the lhs values,  $I_{W'_{1,5}}$  and  $I_{W'_{2,5}}$ , obtained by integrating over the  $R$ -ratio data:

$$I_{W'_{1,5}}(\text{lhs}) = 0.4788(16), \\ I_{W'_{2,5}}(\text{lhs}) = 0.08922(34). \quad (3.9)$$

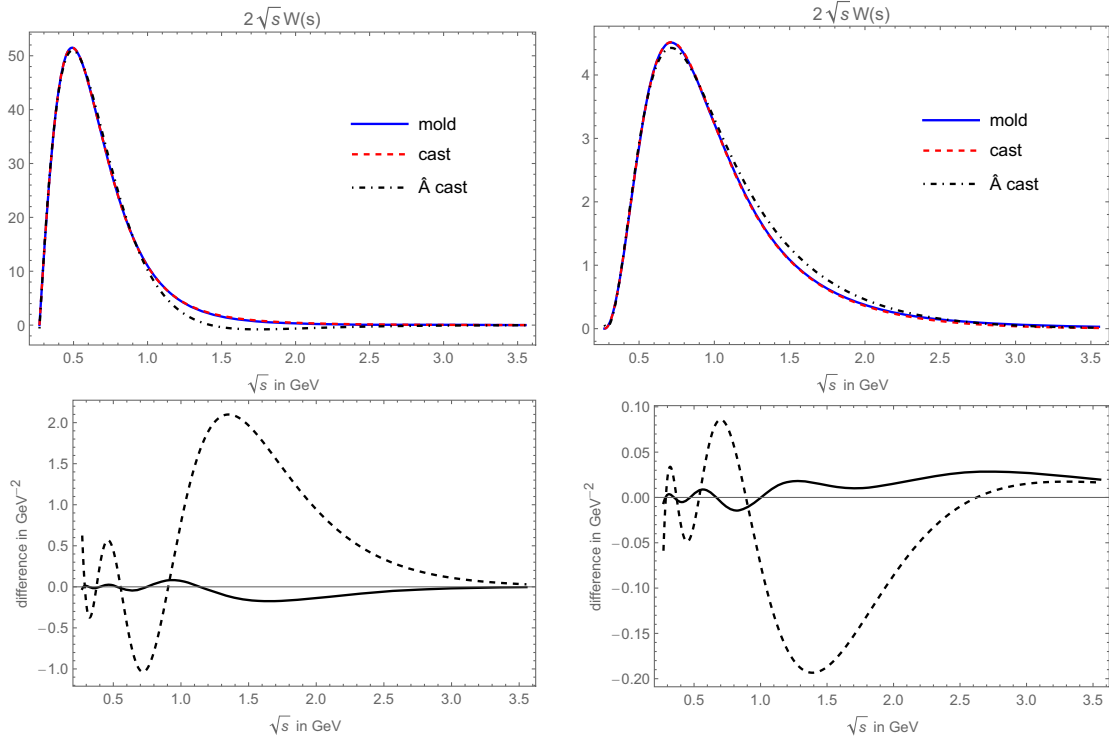


FIG. 4. Upper panels: molds (blue continuous curves) and casts (red dashed curves) for the molds  $2\sqrt{s}W_{1,5}(s)$  (left panel) and  $2\sqrt{s}W_{2,5}(s)$  (right panel). The black dot-dashed curves show the casts obtained with  $\hat{A}$  of Eq. (2.21) instead of  $A$  of Eq. (2.20), choosing  $\lambda = 10^{-9}$ . Lower panels: differences between mold and cast, for each case (with the dashed curves the difference for the  $\hat{A}$ -based casts). Note the very different scales on the vertical axes in the upper and lower figures.



TABLE II. The right-hand side of Eq. (2.18) for the lattice ensembles of Ref. [33]. The second and third columns give, respectively, the values for  $I_{W'_{1.5}}$  and  $I_{W'_{2.5}}$ , obtained using Eq. (3.11). The fourth and fifth columns give, respectively, the values for  $I_{\hat{W}_{1.5}}$  and  $I_{\hat{W}_{2.5}}$ , obtained using  $\hat{A}$  of Eq. (2.21) instead of  $A$ , with  $\lambda = 10^{-9}$ . Below the blank line we show (i) the continuum extrapolation for each column, obtained using fits linear in  $a^2$  to the values for the first three ensembles (96, 64 and 48I), (ii) the  $p$ -value of that fit, and (iii) the relative statistical error (Rel. error) of the continuum limit value.

Label	$I_{W'_{1.5}}$ (rhs)	$I_{W'_{2.5}}$ (rhs)	$I_{\hat{W}_{1.5}}$ (rhs)	$I_{\hat{W}_{2.5}}$ (rhs)
96	0.504(20)	0.0799(23)	0.4625(75)	0.0838(12)
64	0.4822(92)	0.08703(94)	0.4520(38)	0.08994(54)
48I	0.4790(72)	0.09187(80)	0.4401(40)	0.09558(51)
32	0.498(12)	0.10073(76)	0.4398(68)	0.10623(45)
48II	0.4837(85)	0.1009(11)	0.4301(46)	0.10605(64)
$a = 0$	0.496(17)	0.0798(18)	0.4669(68)	0.0824(10)
$p$ -value	0.44	0.15	0.78	0.10
Rel. error	3.4%	2.2%	1.5%	1.2%

For  $I_{\hat{W}_{1.5}}$  and  $I_{\hat{W}_{2.5}}$  we find

$$\begin{aligned} I_{\hat{W}_{1.5}}(\text{lhs}) &= 0.4488(16), \\ I_{\hat{W}_{2.5}}(\text{lhs}) &= 0.09214(37). \end{aligned} \quad (3.10)$$

As before, the  $R$ -ratio data of Ref. [11] allow us to determine these values with errors  $\lesssim 0.4\%$ . We note that the values in Eq. (3.9) or (3.10) are not the same as those in Eq. (3.2), even if they are rather close. This reflects the fact that mold and cast weights are not identical.

Because of the well-known even-odd time oscillation of staggered correlators, we define smoothed-out correlators

$$\hat{C}(t) = \frac{1}{4}(C(t-1) + 2C(t) + C(t+1)). \quad (3.11)$$

We will use the averaged correlator  $\hat{C}(t)$  when evaluating the rhs of Eq. (2.18).<sup>7</sup>

We show the results for  $I_{W'_{1.5}}$  (rhs),  $I_{W'_{2.5}}$  (rhs),  $I_{\hat{W}_{1.5}}$  (rhs) and  $I_{\hat{W}_{2.5}}$  (rhs) in Table II. Using the values obtained with the three smallest lattice spacings, i.e., the ensembles 96, 64 and 48I, and performing fits linear in  $a^2$ , we find the continuum-limit values

$$\begin{aligned} I_{W'_{1.5}}(\text{rhs}) &= 0.496(17), \\ I_{W'_{2.5}}(\text{rhs}) &= 0.0798(18), \end{aligned} \quad (3.12)$$

and

<sup>7</sup>More sophisticated approaches are possible, but we consider this average sufficient for the explorative nature of this section.

$$\begin{aligned} I_{\hat{W}_{1.5}}(\text{rhs}) &= 0.4669(68), \\ I_{\hat{W}_{2.5}}(\text{rhs}) &= 0.0824(10). \end{aligned} \quad (3.13)$$

These linear fit results are shown by the red lines in Fig. 5. The blue curves in the same figure show the results of alternate fits quadratic in  $a^2$  obtained using the four ensembles 96, 64, 48I and 48II. The linear and quadratic fits give consistent continuum-limit results.

As shown in the Table II, the integrals,  $I_{W'_{1.5}}$  (rhs) and  $I_{W'_{2.5}}$  (rhs) in Eq. (3.12) have precisions of 3.4% and 2.2%, respectively, while  $I_{\hat{W}_{1.5}}$  (rhs) and  $I_{\hat{W}_{2.5}}$  (rhs) in Eq. (3.13) have precisions of 1.5% and 1.2%, respectively. We see that the modification (2.21) indeed pays off. We emphasize again that the lhs and rhs central values should not be directly compared in this study. What is of interest here is the size of the statistical errors in Eqs. (3.9), (3.10), (3.12), and (3.13). While those in Eqs. (3.9) and (3.10) are the same as those in Eq. (3.2), those in Eqs. (3.12) and (3.13) are significantly smaller than those in Eq. (3.3). This reflects the freedom to avoid, through the restricted set of  $t_j$  values employed in Eqs. (3.12) and (3.13), higher-error, large- $t$  contributions, and provides a concrete example of the potential enhanced utility of EWSRs over their closely related RWSR counterparts.

The improvement represented by the EWSR construction is, of course, expected to vary depending on the choice of the  $\{t_j\}$  and the strategy chosen for obtaining the associated coefficients  $\{x_j\}$ . We have already seen that, for the set of  $\{t_j\}$  chosen above, using the strategy of Eq. (2.21) produces generally smaller  $\{x_j\}$  and hence, as a result of reduced cancellation, improved errors on the lattice sides of the associated EWSRs. We thus expect other strategies for constructing EWSR weights which limit the size of the  $\{x_j\}$  to also produce EWSRs with reduced lattice-side relative errors. Such considerations suggest, e.g., avoiding sets  $\{t_j\}$  in which the  $t_j$  are too closely spaced since reducing the spacing between adjacent  $t_j$ , in reducing the difference between the associated basis functions  $E^2 \exp(-t_j E)$ , is likely to force an increase in the size of the associated coefficients  $\{x_j\}$ .<sup>8</sup>

We add several comments. First, it is likely that lattice data in the near future will have smaller statistical errors than does the lattice data of Ref. [33], used in the current study. This makes it not unlikely that sub-percent precision can be reached with EWSRs. Second, we did not discuss

<sup>8</sup>An example of the impact of choosing an overly finely spaced set  $\{t_j\}$  is provided by EWSRs based on alternate versions,  $W''_{15}$  and  $W''_{25}$ , of the primed weights above, obtained using the more finely spaced set,  $\{t_j\} = \{3, 5, 7, 9, 11, 13, 15\}$  GeV<sup>-1</sup>, covering the same range in  $t$  as the set (3.4). This finer spacing produces relative errors on the lattice sides of  $W''_{15}$  and  $W''_{25}$  EWSRs of 3.5% and 3.3%, respectively, which represents a 50% error increase in the case of  $W''_{25}$  when compared with the results of Table II.

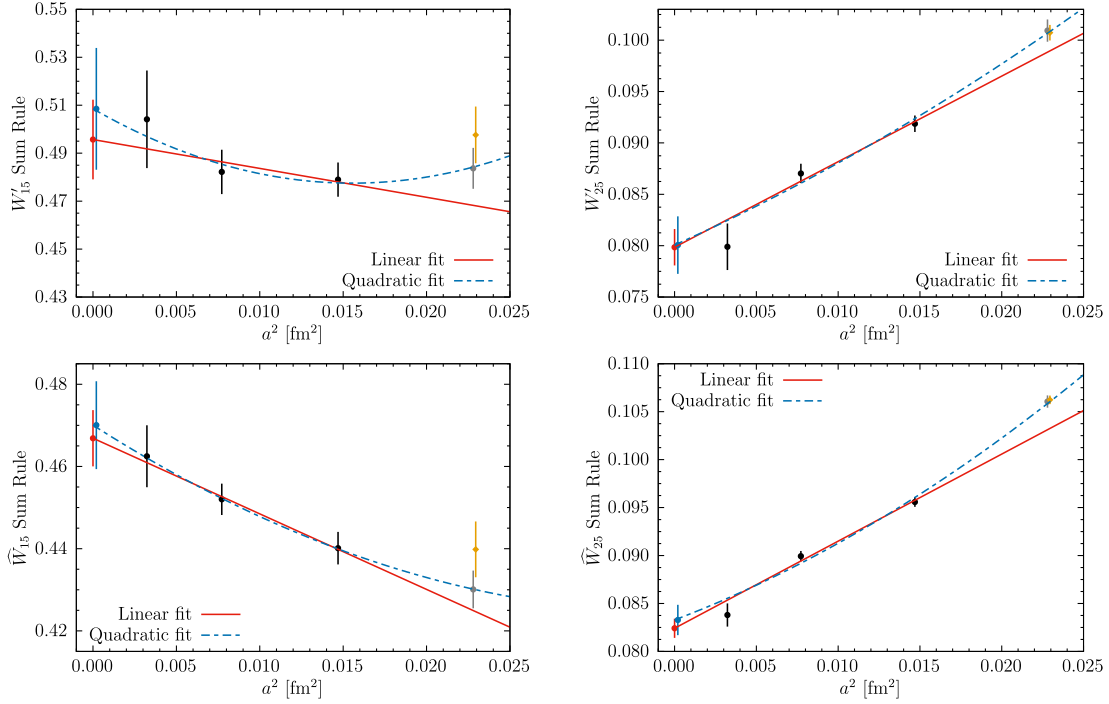


FIG. 5. Continuum extrapolations of  $I_{W'_{1.5}}$  (rhs) (left upper panel) and  $I_{W'_{2.5}}$  (rhs) (right upper panel), and  $I_{\widehat{W}_{1.5}}$  (rhs) (left lower panel) and  $I_{\widehat{W}_{2.5}}$  (rhs) (right lower panel). The data points show the lattice results for the various ensembles. Linear fits to the three left-most points (omitting the gray filled circles) are shown by the red lines, and quadratic fits to all four data points (the black and gray filled circles) by the dashed blue curves. Results for the 32 ensemble, shown as orange diamonds, are not used in either of these extrapolations.

systematic errors, which of course also need to be controlled. In particular, for staggered fermions, smaller lattice spacings than the current smallest value of about 0.06 fm will be needed [33]. We thus do not claim that our linear fits to the results in Table II are the final word. However, similar fits to improved data at smaller lattice spacings should allow these sum rules to become of practical use. Finally, we note that the  $W_{1.5}$  versions of Eqs. (3.9) and (3.12) are closer together than the  $W_{2.5}$  versions. This can be qualitatively understood. The large- $t$  part of the full HVP correlator  $C(t)$  with  $j_\mu = j'_\mu$  the hadronic electromagnetic current is dominated by the light-quark-connected part, more so than the smaller- $t$  part. As can be seen from Fig. 2, the weight  $W_{1.5}$  has support at smaller  $s$ . This translates into having support at larger  $t$ , as can be seen in Fig. 3. This explains the closer agreement for the  $W_{1.5}$ -based case. A similar observation also holds for Eqs. (3.2) and (3.3) in Sec. III A.

### C. Comparison with BABAR-KLOE discrepancy

One would like to get an idea about what is needed to make the lattice errors in Eq. (3.12) small enough for concrete applications of these sum rules. To this end, we consider, as an example, the difference of the values of  $I_{W'_{1.5}}$  and  $I_{W'_{2.5}}$  computed using the BABAR [51,52] or KLOE [53] versions of the two-pion contribution to the EM

spectral function. As Ref. [53] provides the  $e^+e^- \rightarrow \pi^+\pi^-$  cross sections only up to  $s = 0.95 \text{ GeV}^2$ , we will assume that the full discrepancy originates from the difference in the measured cross sections below  $s = 0.95 \text{ GeV}^2$ . This allows us to evaluate the two-pion contributions to  $I_{W_{1/2.5}}$ ,  $I_{W'_{1/2.5}}$  and  $I_{\widehat{W}_{1/2.5}}$  on both the BABAR and KLOE data. We find

$$\begin{aligned}
 I_{W_{1.5}}^{\pi\pi}(\text{BABAR}) - I_{W_{1.5}}^{\pi\pi}(\text{KLOE}) &= 0.0091(39), \\
 I_{W_{2.5}}^{\pi\pi}(\text{BABAR}) - I_{W_{2.5}}^{\pi\pi}(\text{KLOE}) &= 0.00152(51), \\
 I_{W'_{1.5}}^{\pi\pi}(\text{BABAR}) - I_{W'_{1.5}}^{\pi\pi}(\text{KLOE}) &= 0.0091(39), \\
 I_{W'_{2.5}}^{\pi\pi}(\text{BABAR}) - I_{W'_{2.5}}^{\pi\pi}(\text{KLOE}) &= 0.00153(52), \\
 I_{\widehat{W}_{1.5}}^{\pi\pi}(\text{BABAR}) - I_{\widehat{W}_{1.5}}^{\pi\pi}(\text{KLOE}) &= 0.0094(40), \\
 I_{\widehat{W}_{2.5}}^{\pi\pi}(\text{BABAR}) - I_{\widehat{W}_{2.5}}^{\pi\pi}(\text{KLOE}) &= 0.00150(51). \quad (3.14)
 \end{aligned}$$

Comparing these values with the lattice values of Eqs. (3.12) and (3.13), we see that the lattice errors are factors of about 1.9, 1.2, 0.7 and 0.7 times the differences shown in Eq. (3.14) for  $W'_{1.5}$ ,  $W'_{2.5}$ ,  $\widehat{W}_{1.5}$  and  $\widehat{W}_{2.5}$ , respectively. This implies that in order to use the EWSRs with the primed weights, an improvement of a factor about 2 to 4 in the lattice errors would be needed, while for the hatted weights, a very modest improvement

would be sufficient for the EWSRs to weigh in on the *BABAR*-KLOE discrepancy. A combination of more precise lattice data and possibly a more fine-tuned design of the sum-rule weight functions would help accomplishing this. We note that, for this goal, the weight  $W'_{2,5}$  was better “designed” than the weight  $W'_{1,5}$ , and the weight  $\hat{W}_{2,5}$  similarly better “designed” than the weight  $\hat{W}_{1,5}$ . We also note that, in both cases, the hatted weights outperform their primed counterparts.

#### IV. USING HADRONIC $\tau$ -DECAY DATA FOR $a_\mu^{\text{HVP}}$

We now turn to a different application of the sum rules introduced in Sec. II: the use of spectral data obtained from nonstrange vector-current-induced hadronic  $\tau$ -decay data in the determination of  $a_\mu^{\text{HVP}}$ .

The idea of using  $\tau$  data is straightforward in the isospin limit. If isospin were an exact symmetry, one could replace contributions to the  $R$ -ratio from  $I = 1$  exclusive modes in  $e^+e^- \rightarrow$  hadrons by the corresponding contributions implied by the conserved vector current relation and the related vector-channel ( $G$ -parity positive) exclusive-mode hadronic  $\tau$ -decay distributions, for  $s \leq m_\tau^2$ . Doing so is potentially useful for three reasons: (i) if, for a certain energy region, the  $\tau$  data are more precise, this would help in improving the precision of the dispersive determination of  $a_\mu^{\text{HVP}}$ ; (ii) the  $\tau$  data might shed light on the long-standing discrepancy between *BABAR* and KLOE results for the  $e^+e^- \rightarrow \pi^+\pi^-$  cross sections observed in the  $\rho$  region discussed in Sec. III C; and (iii) likewise, the  $\tau$  data might shed light on the increasing evidence for discrepancies between  $R$ -ratio and lattice based evaluations of  $a_\mu^{\text{HVP}}$  or closely related window quantities.

One of the reasons the current best dispersive determination of  $a_\mu^{\text{HVP}}$  does not employ hadronic  $\tau$ -decay data is that, in the real world, isospin is broken by electromagnetic corrections and the difference in up and down quark masses. Typically, both isospin-breaking (IB) effects are expected to be of order a percent or so (except possibly in the region of narrow interfering resonances, where the effects may be larger). Given the precision with which  $a_\mu^{\text{HVP}}$  is obtained in the dispersive approach, IB effects thus need to be brought under quantitative control. Models for IB have been employed in the past [3], but these are not under full phenomenological control, as evidenced by the fact that they fail to account for the observed differences between the experimental  $\tau$  and electroproduction  $\pi\pi$  distributions (see, for example, Figs. 20 and 22 of Ref. [3]). Because of the steady improvement in  $R$ -ratio data, and the problem of achieving an understanding of the IB corrections one needs to apply to the  $\tau$   $\pi\pi$  data, recent high-precision dispersive estimates of  $a_\mu^{\text{HVP}}$  do not involve  $\tau$ -decay data at all.

There are, nevertheless, several reasons to revisit this topic. First, lattice QCD may be able to produce relevant,

first-principle, estimates for IB effects that are useful in the comparison between  $e^+e^-$ -based and  $\tau$ -based data, as will be discussed below. Second, a new combination of the sum of the  $\pi^-\pi^0$ ,  $2\pi^-\pi^+\pi^0$  and  $\pi^-3\pi^0$  contributions to the isovector, vector spectral function from ALEPH and OPAL data has recently been obtained, producing an at-present-best publicly available result for the sum of the contributions from these modes [46].<sup>9</sup> Significant further improvements to the precision for this sum may, moreover, be achievable using Belle II data.<sup>10</sup>

The basic idea is, using the weights  $W_{m,n}$ ,  $W'_{m,n}$  or  $\hat{W}_{m,n}$ , to compare the weighted spectral integrals computed with spectral data obtained from electroproduction and from hadronic  $\tau$  decays. For any (sum of)  $I = 1$  channels, the SM difference is caused by IB, and can be expressed as the corresponding difference of the rhs of Eq. (2.11) [or (2.18)]. In principle, the rhs differences can be computed on the lattice, as we will discuss in Sec. IV A. The other important ingredient is the precision with which the  $W_{m,n}$ ,  $W'_{m,n}$  or  $\hat{W}_{m,n}$ -weighted spectral integrals can be evaluated. As we will see, choosing weights like  $W_{1,5}$  and  $W_{2,5}$ , which zoom in on the region of the *BABAR*-KLOE discrepancy, the weighted spectral integrals of the electroproduction- and  $\tau$ -based data are already sufficiently precise that results using current  $\tau$  data will allow one to weigh in on the *BABAR*-KLOE discrepancy, provided the required IB corrections can be evaluated with comparable precision on the lattice. We will discuss this point more quantitatively in Sec. IV B.

##### A. Isospin breaking

The main problem in comparing spectral data from electroproduction and hadronic  $\tau$  decays using lattice data to compute IB effects in the hadronic vacuum polarization  $\Pi(Q^2)$  is that the lattice can only access  $\Pi(Q^2)$  for Euclidean  $Q^2$ .<sup>11</sup> This is not a problem if one wants to compare fully inclusive results for  $a_\mu^{\text{HVP}}$ , since representations exist for  $a_\mu^{\text{HVP}}$  both as a weighted integral of the  $R$  ratio,  $R(s)$ , over  $s$  [55–57] and as a weighted integral of  $\hat{\Pi}(Q^2)$  over  $Q^2$  [58–60]. It does, however, become a problem if one wants to restrict oneself to contributions from a subset of exclusive modes, and/or to restrict  $s$  to a given region  $s_{\min} \leq s \leq s_{\max}$ . Because of the kinematic

<sup>9</sup>The reason only the sum is available is that the ALEPH and OPAL covariance matrices for the two  $4\pi$  distributions are highly singular, which can lead to biased results in the data-combination procedure. The sum of  $2\pi$  and  $4\pi$  contributions has a much better behaved covariance matrix and avoids this issue.

<sup>10</sup>An additional practical issue is the need to ensure the radiative corrections applied to  $\tau$  data match those employed in the analysis of electroproduction data. For more on this issue, and work in progress on evaluating the relevant corrections, see Ref. [54].

<sup>11</sup>Or, equivalently,  $C(t)$  for Euclidean  $t$ .

restriction  $s \leq m_\tau^2$  for  $\tau$  decays,  $s_{\max}$  by necessity has to be chosen  $\leq m_\tau^2$ , whereas one may want to choose  $s_{\min}$  larger than threshold to reduce the relative statistical errors. Similar observations apply to the sum rules of Sec. II, in which, as for  $a_\mu^{\text{HVP}}$ , the spectral integrals are evaluated from  $s_{\text{th}}$  to  $\infty$ .

The bulk of the dispersive contributions to  $a_\mu^{\text{HVP}}$  come from electroproduction data below  $\sqrt{s} = 1.937$  GeV, with  $e^+e^- \rightarrow 2\pi, 3\pi, 4\pi$  and  $K\bar{K}$  accounting for 72.8%, 6.7%, 4.9% and 5.2%, respectively, for a total of 89.7%, according to Ref. [111].

Contributions from all other exclusive modes below  $\sqrt{s} = 1.937$  GeV represent a further 2.6%, those from narrow charm and bottom resonances a further 1.1%, those from inclusive  $R(s)$  data between  $\sqrt{s} = 1.937$  and 11.199 GeV a further 6.3%, and those [evaluated using perturbative QCD (pQCD)] from  $\sqrt{s}$  above 11.199 GeV a further 0.3%. The contributions from the  $2\pi, 3\pi, 4\pi$  and  $K\bar{K}$  exclusive modes below  $\sqrt{s} = 1.937$  GeV, similarly, represent 98% and 89%, respectively, of the full spectral integrals  $I_{W_{1,5}}$  and  $I_{W_{2,5}}$ .

With contributions from the remaining exclusive modes below  $\sqrt{s} = 1.937$  GeV lying at  $s$  far removed from narrow interfering resonances which might enhance IB, it seems reasonable to expect IB in these residual exclusive-mode contributions to be very small. We estimate these as of order 1% of the 2.6% total contribution from these modes.

In the region above  $\sqrt{s} = 1.937$  GeV, away from the narrow charm and bottom resonances, the experimental  $R(s)$  data used in obtaining the 6.3% inclusive-region contribution of Ref. [11] agrees with pQCD expectations to significantly better than 10%. With IB corrections well below 1% in the OPE representation of  $\rho_{\text{EM}}(s)$ , estimating possible IB contributions from the region above  $\sqrt{s} = 1.937$  GeV as less than 1% of the 7.7% total from this region should represent a very conservative assessment.

With the 1% or less estimates discussed above for IB in both the contributions from exclusive modes other than  $2\pi, 3\pi, 4\pi$  and  $K\bar{K}$  below  $\sqrt{s} = 1.937$  GeV and all contributions in the region above  $\sqrt{s} = 1.937$  GeV, we conclude that IB contributions from these sources should represent less than 0.1% of the total for  $a_\mu^{\text{HVP}}$ ; a similar conclusion holds for  $I_{W_{1,5}}$  and  $I_{W_{2,5}}$ . In summary, since the contributions from channels other than  $2\pi, 3\pi, 4\pi$  and  $K\bar{K}$  below  $\sqrt{s} = 1.937$  GeV and all contributions in the region above  $\sqrt{s} = 1.937$  GeV represent less than 11% of the totals for all of  $a_\mu^{\text{HVP}}, I_{W_{1,5}}$  and  $I_{W_{2,5}}$ , and it is safe to estimate IB for these quantities as at most of order 1%, IB contributions should represent of order 0.1% or less of the total for all three quantities. The uncertainty resulting from neglecting such contributions can thus be safely neglected given the present state of the art.

In Ref. [61] it was shown that the IB effect in the  $I = 1$  vector  $K\bar{K}$  channel is expected to be much smaller than the typical few percent of the full  $I = 0 + 1$  sum, because  $\tau$ -decay data for the  $I = 1$  contribution allows one to see that the  $K\bar{K}$  electroproduction cross sections are strongly dominated by the  $I = 0$  contribution from the  $\phi$ -peak region [62]. The IB effects on the small  $I = 1$  part of the  $K\bar{K}$  channel should thus also be negligibly small.

It follows from the analysis of Ref. [61] that, to first order in IB, IB effects for all nonstrange vector-channel  $\tau$  exclusive-mode contributions except those from the  $2\pi$ -pion and  $4\pi$ -pion modes are so small that for the purpose of estimating IB corrections (apart from possible IB effects in the  $e^+e^- \rightarrow 3\pi$  distribution to be discussed in more detail below) a fully inclusive lattice result for

$$\Pi_{\text{IB}}(Q^2) \equiv \frac{2}{\sqrt{3}}\Pi_{38}(Q^2) + \left[ \Pi_{33}(Q^2) - \frac{1}{2}\Pi_{ud;V}(Q^2) \right] \quad (4.1)$$

can be used to correct the sum of  $2\pi$  and  $4\pi$  contributions obtained from non-strange vector-channel hadronic  $\tau$ -decay data, producing an alternate, combined  $\tau$ -plus-lattice-IB determination for the sum of  $\pi^+\pi^-, 2\pi^+2\pi^-$  and  $\pi^+\pi^-2\pi^0$  electroproduction contributions.<sup>12</sup>

From the above discussion, it follows, using Eq. (2.9), again up to possible IB contributions in the  $e^+e^- \rightarrow 3\pi$  distribution which, to first order in IB, would produce unwanted 3-pion contributions to the mixed-isospin,  $ab = 38$  part of  $\rho_{\text{EM}}(s)$ , and hence also to  $\Pi_{38}(Q^2)$  in Eq. (4.1), that

$$\begin{aligned} \Delta_{m,n} &\equiv \int_{s_{\text{th}}}^{s_{\text{KNT}}} ds W_{m,n}(s; \{Q_\ell^2\}) \rho_{2\pi+4\pi}^{e^+e^-}(s) \\ &\quad - \int_{s_{\text{th}}}^{s_{\text{KNT}}} ds W_{m,n}(s; \{Q_\ell^2\}) \rho_{2\pi+4\pi}^\tau(s), \\ &= (-1)^m m_\tau^{2(n-m-1)} \sum_{k=1}^n \frac{(Q_k^2 + s_{\text{th}})^m}{\prod_{\ell \neq k} (Q_\ell^2 - Q_k^2)} \Pi_{\text{IB}}(Q_k^2), \end{aligned} \quad (4.2)$$

where  $s_{\text{KNT}} = (1.937 \text{ GeV})^2$  is the upper edge of the exclusive-mode data region of Ref. [11],  $\rho_{2\pi+4\pi}^{e^+e^-}$  is the sum of the  $2\pi$  and  $4\pi$  contributions to the electromagnetic current spectral function implied by  $2\pi$  and  $4\pi$  electroproduction cross sections and  $\rho_{2\pi+4\pi}^\tau$  is the sum of the  $2\pi$  and  $4\pi$  contributions to the consistently normalized vector  $I = 1$  spectral function implied by nonstrange vector-current-induced hadronic  $\tau$  decay distribution results. Alternate versions of this sum rule in terms of  $C_{\text{IB}}(t)$  [cf. Eqs. (2.11) or (2.18)] can of course also be employed. We will discuss the feasibility of this through concrete

<sup>12</sup>A preliminary lattice study of some of the contributions to Eq. (4.1) already exists [54,63].

examples in Sec. IV B, where we will evaluate the lhs of Eq. (4.2) for the weights  $W_{1,5}$  and  $W_{2,5}$  using data from Refs. [11,46].

We now return to the issue of possible nontrivial IB effects in the  $e^+e^- \rightarrow 3\pi$  distribution, which complicates the process of identifying the exclusive-mode contributions in the dispersive integral over the electroproduction data to be replaced by lattice-IB-corrected  $\tau$  results. This complication arises because there may be 3-pion exclusive-mode contributions to the spectral function of the mixed-isospin  $\Pi_{38}$  polarization. In the isospin limit, the  $3\pi$  mode is pure  $I = 0$ , and thus not affected by the replacement of part of the  $I = 1$  component of the electromagnetic spectral function by the corresponding part of the vector-channel,  $I = 1$   $\tau$  spectral function. With IB, however, the 38 part of Eq. (4.1) will contain a 3-pion contribution, with  $\rho - \omega$  mixing, for example, inducing a contribution to the 38 spectral function via  $e^+e^- \rightarrow \rho \rightarrow \omega \rightarrow 3\pi$ . Applying the inclusive lattice IB correction to the weighted  $\tau$   $2\pi + 4\pi$  integral and using the result to replace the corresponding  $2\pi + 4\pi$  contribution to the weighted electroproduction integral, the modified all-exclusive-mode sum would then include this  $3\pi$  IB component twice, once in the inclusive lattice IB correction, and once in the  $3\pi$  contribution produced by use of the experimental  $e^+e^- \rightarrow 3\pi$  cross sections. The result of Ref. [11] for the contribution of the  $3\pi$  channel to  $a_\mu^{\text{HVP}}$ ,  $46.73(94) \times 10^{-10}$ , is sufficiently large that, were the associated IB  $3\pi$  contribution to be larger than naively expected, say at a level a few to several percent of the full  $3\pi$  contribution, a controlled estimate of its size might be required to make an inclusive lattice  $\Pi_{\text{IB}}(Q^2)$  determination, however precise, of actual numerical use in performing an IB correction of  $\tau$ -decay data.

Fortunately, experimental information is now available on what should be the dominant contribution to this  $3\pi$  double counting, with recent *BABAR* results [64] providing  $>6\sigma$  evidence for an IB  $e^+e^- \rightarrow \rho \rightarrow 3\pi$  contribution to the  $e^+e^- \rightarrow 3\pi$  amplitude. The interference of this contribution with the isospin-conserving (IC)  $e^+e^- \rightarrow \omega \rightarrow 3\pi$ ,  $e^+e^- \rightarrow \phi \rightarrow 3\pi$ ,  $e^+e^- \rightarrow \omega' \rightarrow 3\pi$  and  $e^+e^- \rightarrow \omega'' \rightarrow 3\pi$  contributions produces IB contributions to the cross section, and hence IB contributions to the weighted integrals over the  $3\pi$  distribution involving the weights discussed in this paper. The normalization of these interference contributions is fixed by the square root of the fitted  $\rho \rightarrow 3\pi$  branching fraction,  $B(\rho \rightarrow 3\pi)$ , to which these contributions are proportional. Taking the integrals up to the upper edge,  $s = (1.937 \text{ GeV})^2$ , of the KNT19 exclusive-mode region to be specific, the IB contributions implied by the preferred *BABAR* cross-section fit, as detailed in Appendix B, turn out to represent  $-1.2(1.2)\%$ ,  $-1.1(1.1)\%$  and  $-1.6(1.6)\%$  of the corresponding full  $3\pi$  contributions to  $a_\mu^{\text{HVP}}$ ,  $I_{W_{1,5}}$  and  $I_{W_{2,5}}$ , respectively.

In the  $a_\mu^{\text{HVP}}$  case, the resulting  $3\pi$ -double-counting correction,  $+0.54(0.54) \times 10^{-10}$  [from Eq. (B1)], represents  $+0.08(0.08)\%$  of the  $a_\mu^{\text{HVP}}$  total. At present, a  $\pm 0.54 \times 10^{-10}$  uncertainty on the  $\tau$ -modified alternate determination of  $a_\mu^{\text{HVP}}$  is sufficiently small that replacing electroproduction data by  $\tau$ -based data for the  $2\pi$  and  $4\pi$  channels is potentially useful for the purposes of investigating, for example, the *BABAR*-*KLOE* discrepancy, where the discrepancy between *BABAR* and *KLOE*  $2\pi$  contributions from the region  $0.6 \text{ GeV} < \sqrt{s} < 0.9 \text{ GeV}$  [11],  $(9.8 \pm 3.5) \times 10^{-10}$ , is much larger than the  $3\pi$  double-counting-correction uncertainty. In Sec. IV B we will show that a similar conclusion holds for the  $W_{1,5}$  and  $W_{2,5}$  weight cases: the  $\pm 0.00041$  and  $\pm 0.00012$  uncertainties on the  $W_{1,5}$  and  $W_{2,5}$   $3\pi$ -double-counting corrections obtained in Appendix B are once more much smaller than the central values and experimental errors on the corresponding electroproduction- $\tau$  spectral integral differences.

A more detailed discussion of the IB contributions to the weighted  $3\pi$  integrals may be found in Appendix B.

## B. Comparison of $\tau$ -based and $e^+e^-$ -based spectral integrals

We now turn to the evaluation of the  $2\pi + 4\pi$  contributions to the spectral integrals appearing in Eq. (4.2), for the examples  $W_{m,n} = W_{1,5}$  and  $W_{2,5}$ . The  $2\pi + 4\pi$  data of Ref. [11] is used in the first integral and that of Ref. [46] in the second integral. We also consider the  $3\pi$  channel, in view of the discussion at the end of Sec. IV A. The discussion is restricted to contributions from the exclusive-mode region of Ref. [11],  $s \leq s_{\text{KNT}} = (1.937 \text{ GeV})^2$ , since  $2\pi$ ,  $3\pi$  and  $4\pi$  contributions above that point form part of the multimode inclusive contribution, dealt with already in Sec. IV A. Since no lattice data is currently available to evaluate the rhs of either Eq. (4.2) or its EWSR analog, we restrict our attention to the  $W_{1,5}$  and  $W_{2,5}$  RWSR examples, and do not consider the EWSR analogs. Once suitable IB lattice data become available, the analogous EWSR cases may become of interest, for the reasons explained in Sec. III B.

Our goal here is to see whether the two integrals on the lhs of Eq. (4.2) can be evaluated with sufficient precision to make this sum rule of potential use. Of relevance to investigating this question is the size of the uncertainty on the spectral integral differences appearing on the lhs of Eq. (4.2) relative to (i) the uncertainties on estimates for the corresponding  $3\pi$ -double-counting corrections, and (ii) variations in the spectral integral differences themselves, induced, for example, by the *BABAR*-*KLOE*  $\pi\pi$  discrepancy.

We start with the electroproduction-based  $W_{1,5}$ - and  $W_{2,5}$ -weighted integrals over the  $2\pi$ ,  $3\pi$  and  $4\pi$  contributions to  $\rho_{\text{EM}}(s)$ , results for which are shown in Table III. We use  $s_{\text{th}} = 4m_\pi^2$ .

TABLE III. Electroproduction-based exclusive-mode spectral integrals with weights  $W_{1.5}$  (left of the double vertical line) and  $W_{2.5}$  (right of the double vertical line). The second and fifth columns show the integrals computed up to  $s = s_{\text{KNT}} = (1.937 \text{ GeV})^2$ , the third and sixth columns the same integrals computed up to  $s = s_\tau = 3.0574 \text{ GeV}^2$ .

Channel	$I_{W_{1.5}}(s_{\text{KNT}})$	$I_{W_{1.5}}(s_\tau)$	$\frac{I_{W_{1.5}}(s_\tau)}{I_{W_{1.5}}(s_{\text{KNT}})}$	$I_{W_{2.5}}(s_{\text{KNT}})$	$I_{W_{2.5}}(s_\tau)$	$\frac{I_{W_{2.5}}(s_\tau)}{I_{W_{2.5}}(s_{\text{KNT}})}$
$\pi^+\pi^-$	0.3864(14)	0.3863(14)	1.00	0.05713(19)	0.05710(19)	1.00
$2\pi^+2\pi^-$	0.005743(81)	0.005450(77)	0.95	0.003568(49)	0.003267(45)	0.92
$\pi^+\pi^-2\pi^0$	0.00813(33)	0.00772(32)	0.95	0.00464(19)	0.00422(17)	0.91
$2\pi + 4\pi$	0.4002(14)	0.3995(14)	1.00	0.06534(27)	0.06459(26)	0.99
$\pi^+\pi^-\pi^0$	0.03880(81)	0.03877(81)	1.00	0.00798(15)	0.00794(15)	1.00

The data files containing the exclusive-mode contributions to  $R(s)$  provided by the authors of Ref. [11] extend up to  $s = s_{\text{KNT}} = 3.7520 \text{ GeV}^2$ . Results for the exclusive-mode,  $s_{\text{KNT}}$ -truncated  $X = \pi^+\pi^-, 2\pi^+2\pi^-, \pi^+\pi^-2\pi^0$  and  $\pi^+\pi^-\pi^0$ ,  $W_{1.5}$ - and  $W_{2.5}$ -weighted spectral integrals obtained using this input, are denoted  $I_{W_{1.5}}^X(s_{\text{KNT}})$  and  $I_{W_{2.5}}^X(s_{\text{KNT}})$  in what follows, and listed in columns 2 and 5 of Table III.

The upper endpoints of the  $\tau$ -based spectral integrals are, in contrast, limited by the largest  $s$  for which the  $\tau$ -based spectral function of Ref. [46] is available, which is  $s \equiv s_\tau = 3.0574 \text{ GeV}^2$ , slightly below  $m_\tau^2$ . To compare to the resulting  $s_\tau$ -truncated  $\tau$ -based integrals, we thus also require values for  $s_\tau$ -truncated versions of the exclusive-mode electroproduction-based integrals. These are denoted  $I_{W_{1.5}}^X(s_\tau)$  and  $I_{W_{2.5}}^X(s_\tau)$  and listed in columns 3 and 6 of Table III. As can be seen from the table, the  $s_\tau$ -truncated integrals constitute more than 99% of the corresponding  $s_{\text{KNT}}$ -truncated versions for the  $2\pi$  and  $3\pi$  modes and more than 90% of the  $s_{\text{KNT}}$ -truncated versions for the two  $4\pi$  modes.

The  $s_\tau$ -truncated  $2\pi + 4\pi$   $\tau$ -based integrals to be compared to the  $R$ -ratio-based analogs of Table III are obtained using the  $2\pi + 4\pi$   $\tau$ -based spectral function of Ref. [46]. The results,

$$\begin{aligned} I_{W_{1.5}}^{\tau, 2\pi+4\pi}(s_\tau) &= 0.4103(22), \\ I_{W_{2.5}}^{\tau, 2\pi+4\pi}(s_\tau) &= 0.06693(22), \end{aligned} \quad (4.3)$$

differ from the electroproduction results of Table III,

$$\begin{aligned} I_{W_{1.5}}^{2\pi+4\pi}(s_\tau) &= 0.3995(14), \\ I_{W_{2.5}}^{2\pi+4\pi}(s_\tau) &= 0.06459(26), \end{aligned} \quad (4.4)$$

by  $4.1\sigma$  and  $6.7\sigma$ , respectively, for the  $W_{1.5}$  and  $W_{2.5}$  cases. The  $s_\tau$ -truncated contributions to the differences appearing on the lhs of the  $W_{1.5}$  and  $W_{2.5}$  versions of Eq. (4.2),

$$\begin{aligned} I_{W_{1.5}}^{2\pi+4\pi}(s_\tau) - I_{W_{1.5}}^{\tau, 2\pi+4\pi}(s_\tau) &= -0.0108(26), \\ I_{W_{2.5}}^{2\pi+4\pi}(s_\tau) - I_{W_{2.5}}^{\tau, 2\pi+4\pi}(s_\tau) &= -0.00233(35), \end{aligned} \quad (4.5)$$

are thus determined with  $\sim 24\%$  and  $\sim 15\%$  precision. We note that the errors in Eq. (4.5) are significantly smaller than the central values of the *BABAR*-*KLOE* discrepancies in Eq. (3.14). The analogous values for  $a_\mu^{\text{HVP}}$  itself are

$$\begin{aligned} a_\mu^{2\pi+4\pi}(s_\tau) &= 535.0(2.0) \times 10^{-10}, \\ a_\mu^{\tau, 2\pi+4\pi}(s_\tau) &= 552.4(5.0) \times 10^{-10}, \\ a_\mu^{2\pi+4\pi}(s_\tau) - a_\mu^{\tau, 2\pi+4\pi}(s_\tau) &= -17.4(5.4) \times 10^{-10}. \end{aligned} \quad (4.6)$$

We comment on the  $\tau$ -based value in Eq. (4.6) (i.e., the second line of this equation). The  $\tau$ -based data are very sparse near the 2-pion threshold end of the spectral function, and a comparison with the  $R$ -ratio-based data (which are much denser in the threshold region) suggests that the trapezoidal interpolation of the  $\tau$ -based data may overestimate the near-threshold,  $\tau$ -based contribution to  $a_\mu^{\tau, 2\pi+4\pi}(s_\tau)$ . A rough estimate of this effect can be obtained by replacing the contribution to  $a_\mu^{\tau, 2\pi+4\pi}(s_\tau)$  between threshold and  $s_{\text{ChPT}} \equiv s = (0.305 \text{ GeV})^2$  by the chiral perturbation theory (ChPT)-based 2-pion contribution from Ref. [11], and then employing trapezoidal integration above  $s_{\text{ChPT}}$ . Doing so would lead to a downward shift of  $0.90(42) \times 10^{-10}$  of the value  $552.4(5.0) \times 10^{-10}$  in Eq. (4.6). This small additional near-threshold uncertainty in the  $\tau$  result for  $a_\mu^{2\pi+4\pi}$  is a consequence of the enhancement of low- $s$  contributions by the  $a_\mu^{\text{HVP}}$  kernel. The weights  $W_{1.5}$  and  $W_{2.5}$ , in contrast, produce no such low- $s$  enhancement (and in fact strongly suppress near-threshold contributions). The uncertainty in the low- $s$   $\tau$ -based  $2\pi$  spectral distribution resulting from the coarseness of the  $\tau$  data near threshold thus has negligible impact on the results in Eq. (4.3). Since weighted spectral integrals with the weights  $W_{1.5}$  and  $W_{2.5}$  are the main focus of this paper, we do not pursue this issue further here.

Of course, before we can meaningfully compare the  $\tau$ - and electroproduction-based integrals, we need to take the rhs, i.e., the projected lattice-based IB correction, into

account. Since this contribution is inclusive, we have to deal with the fact that the  $s_\tau$ -truncated spectral integrals whose differences we are actually able to determine from data are smaller than the complete spectral integrals. While we have already argued in Sec. IV A that IB contributions from modes other than  $2\pi$  and  $4\pi$  below  $s = s_{\text{KNT}}$ , and from all modes above  $s = s_{\text{KNT}}$ , can be safely neglected, we still need to address the size of possible IB contributions from the  $2\pi$  and  $4\pi$  modes in the region  $s_\tau < s < s_{\text{KNT}}$ . For the  $2\pi$  modes, this is not an issue, as the integrals up to  $s_\tau$  capture essentially the full contribution up to  $s_{\text{KNT}}$  for both weights we consider here. The  $s_\tau$ -truncated  $4\pi$  integrals constitute 95%, respectively, 91–92% of the full  $4\pi$  integrals, for the weights  $W_{1,5}$  and  $W_{2,5}$ . In this high- $s$ ,  $s > s_\tau$  region, we expect IB to be of order 1% of the corresponding  $4\pi$  totals. With this estimate, the IB contribution missed as a result of truncating the  $W_{1,5}$  and  $W_{2,5}$  integrals at  $s = s_\tau$  rather than  $s_{\text{KNT}}$  are expected to be (i) in the  $W_{1,5}$  case, of order 1% of 5%, or 0.05%, of the corresponding full  $s_{\text{KNT}}$ -truncated  $4\pi$  contribution, and hence of order 0.000007, and (ii) in the  $W_{2,5}$  case, of order 1% of 9%, or 0.09%, of the corresponding full  $s_{\text{KNT}}$ -truncated  $4\pi$  contribution, and hence of order 0.000007 as well. These estimated higher- $s$   $2\pi + 4\pi$  IB contribution effects, missed when one considers the differences of electroproduction- and  $\tau$ -based  $2\pi + 4\pi$  integrals only up to  $s = s_\tau$ , are thus more than an order of magnitude smaller than the uncertainties, 0.00041 and 0.00012, on the corresponding  $3\pi$ -double-counting corrections estimated in Appendix B, which are, themselves, significantly smaller than both the central values and experimental errors of the Eq. (4.5) results,  $-0.0108 \pm 0.0026$  and  $-0.00233 \pm 0.00035$ , for the  $W_{1,5}$ - and  $W_{2,5}$ -weighted,  $s = s_\tau$ -truncated experimental electroproduction- $\tau$   $2\pi + 4\pi$  spectral integral differences, indicating that a sufficiently precise lattice determination of the corresponding rhs of Eq. (4.2) will, indeed, make these sum rules useful for investigating current electroproduction- and  $\tau$ -based integral results. It remains of course crucial that a lattice estimate of the inclusive IB correction reach a precision commensurate with the precision with which the spectral integral differences in Eq. (4.5) have been obtained.

## V. CONCLUSIONS

At present, there are several discrepancies in the computation of  $a_\mu^{\text{HVP}}$  that limit our ability to compare a SM-based estimate for  $a_\mu$  with the experimentally measured value. Most recently, a puzzling discrepancy has emerged between data-driven and lattice evaluations of the RBC/UKQCD intermediate window quantity, suggesting that a lattice-based value for  $a_\mu^{\text{HVP}}$  may bring the SM value for  $a_\mu$  much closer to the experimental value. This may confirm the lattice result for  $a_\mu^{\text{HVP}}$  found by the BMW collaboration, which is  $2.1\sigma$  higher than the data-driven value. The

discrepancy for the intermediate window turns out to be about half the total difference between the experimental and SM values for  $a_\mu$ , when for the latter the data-driven white-paper value for  $a_\mu^{\text{HVP}}$  of Ref. [3] is used.

Another discrepancy results from the long-standing difference between the *BABAR* and *KLOE* measured spectral distributions in the two-pion channel, in the region around the  $\rho$  mass. Taking this discrepancy at face value, i.e., considering the difference between the values obtained using either the *BABAR* or the *KLOE* data, leads to a difference of about  $10^{-9}$  in  $a_\mu^{\text{HVP}}$ , which is more than half the difference between the experimental and white-paper values for  $a_\mu$ .

Given this puzzling state of affairs, it is important to develop methods that allow for detailed comparisons, zooming in on specific regions in  $s$ . The sum rules developed in this paper provide a tool for such investigations. The RWSRs of Sec. II A are based on weighted spectral integrals with an adjustable narrow-weight function defined directly as a function of  $s$ . The quantities defined by such sum rules complement the window quantities of Ref. [29], which are defined as a function of Euclidean time, and translate into rather wide windows as a function of  $s$ .<sup>13</sup>

In Sec. II B we modified the RWSR approach by borrowing ideas from Ref. [41], proposing a different set of sum rules, with weight functions that are linear combinations of simple exponential functions of  $\sqrt{s}$ . This class of sum rules has the advantage that the lattice side involves the lattice correlator for the vacuum polarization at a set of Euclidean  $t$  values which are chosen by hand and which hence allow one to avoid contributions from the high- $t$  region, where lattice errors are large. This aids in the optimization of the precision of the lattice side of the sum rule. A key observation is that the weights used for the RWSRs can, moreover, be used as molds to cast the exponential weights, thus retaining the advantage of RWSRs. We note that our goal is not to reconstruct spectral data from the lattice, but rather to compare appropriately weighted, moderately localized versions of existing experimental spectral data with correspondingly weighted lattice data. Our goal is thus simpler than the goal of Ref. [41]. In particular, the casts are not used in any approximations; once a useful cast has been designed, it can be used in an exact EWSR, and the underlying mold discarded. In fact, there is considerable flexibility in designing EWSRs. An example of this flexibility is provided by the hatted weight functions based on Eq. (2.21).

Two key points are worth reiterating here. First, weights  $W(s)$  very similar as functions of  $s$  may produce significantly different relative errors on the lattice sides of the

<sup>13</sup>Our method differs from that of Ref. [38], which attempts to narrow the window as a function of  $s$  by taking linear combinations of windows defined as a function of Euclidean time.

associated EWSRs. And second, given that the sum rules corresponding to different weights are all exact, one is free to choose, from any set of such similar weights, the one that produces the most stringent dispersive-lattice comparison. In the examples explored above, this would be the hatted EWSR weights.

Additional ideas for designing practical exponential weights that are narrow as a function of  $s$ , moreover, almost certainly remain to be explored.

At first glance, it is not obvious that these new methods will be practically useful, as there are reasons to worry that the lattice sides of our sum rules will typically have large errors. To investigate this worry, we studied, in Sec. III, two rational weights,  $W_{1,5}$  and  $W_{2,5}$ , and their exponential cousins, numerically, using data from Ref. [11] on the data side, and from Ref. [33] on the lattice side. We found that especially the exponential weights perform quite well for an investigation of, for example, the *BABAR*-KLOE discrepancy. With the projected increase in the precision of data from the lattice, and with more fine-tuning of the weights of Sec. II B, we believe that the new tools provided in this paper are likely to prove quite useful for the investigation of currently existing discrepancies.

In Sec. IV we applied these ideas in a somewhat different context, the comparison between contributions to  $a_\mu^{\text{HVP}}$  from  $R$ -ratio data and hadronic  $\tau$ -decay data. In the past, such comparisons were difficult to carry out because of the lack of a reliable method for estimating isospin-breaking effects. We derived a sum rule allowing for the comparison between  $R$ -ratio and hadronic  $\tau$ -decay based data in which the required IB effects can, to a good approximation, be obtained from the lattice. In particular, we showed that if the two- and four-pion channels are included in the  $R - \tau$  comparison, IB effects in other channels are small enough that IB effects can be reliably incorporated by an inclusive lattice computation, thus avoiding the difficulties associated with obtaining exclusive data from the lattice. Using the weights of Sec. III, we demonstrated that this comparison can become practical with sufficiently precise lattice data for the inclusive IB correction.

We conclude by emphasizing that this paper is a method paper. The main reason is that we do not have access to lattice data for the complete hadronic vacuum polarization, or for the IB part of it needed in Sec. IV. We have not optimized the concrete examples of Sec. III and Sec. IV for the specific goals for which they may be used. We leave the optimization of these new classes of sum rules to future work, and here just comment that this optimization will depend on the specific application.

### ACKNOWLEDGMENTS

We thank Alex Keshavarzi for making all exclusive-mode data underlying Ref. [11] available to us. We thank Mattia Bruno and Max Hansen for useful discussions, and Marcus V. Rodrigues for his participation at an early stage of this

work. D.B.'s work was supported by the São Paulo Research Foundation (FAPESP) Grant No. 2021/06756-6 and by CNPq Grant No. 308979/2021-4. M. G. is supported by the U.S. Department of Energy, Office of Science, Office of High Energy Physics, under Award No. DE-SC0013682. The work of K. M. is supported by a grant from the Natural Sciences and Engineering Council of Canada. S.P. is supported by the Spanish Ministry of Science, Innovation and Universities (Project No. PID2020-112965 GB-I00/AEI/10.13039/501100011033) and by Grant No. 2017 SGR 1069. I. F. A. E. is partially funded by the CERCA program of the Generalitat de Catalunya.

### APPENDIX A: RELATION BETWEEN WEIGHTS AND PRECISION

Consider the weights of Eq. (2.7), without the extra factors of  $m_\tau$ :

$$W_{m,n}(s) = \frac{(s - s_{\text{th}})^m}{\prod_{k=1}^n (s + Q_k^2)}, \quad (\text{A1})$$

where  $0 < Q_1^2 < Q_2^2 < \dots < Q_n^2$ . What we will discuss in this appendix is the issue of the cancellations involved when this weight is used in the sum-rule approach discussed in the main text.

The function  $W_{m,n}(s)$  can be rewritten in the alternate partial-fraction representation form

$$W_{m,n}(s) = \sum_{k=1}^n \frac{c_k}{(s + Q_k^2)}, \quad (\text{A2})$$

where the  $c_k$  are easily seen to be

$$c_k = \frac{(-1)^m (Q_k^2 + s_{\text{th}})^m}{\prod_{\ell \neq k} (Q_\ell^2 - Q_k^2)}. \quad (\text{A3})$$

By expanding in  $1/s$  for large  $s$ , it is straightforward to work out a number of relations satisfied by the  $c_k$ , as follows. In the form Eq. (A1), it is clear that

$$W_{m,n}(s) = \frac{1}{s^{n-m}} + \mathcal{O}\left(\frac{1}{s^{n-m+1}}\right), \quad (\text{A4})$$

where the expansion is convergent for  $s > Q_N^2$ . In contrast, expanding the form Eq. (A2), the large  $s$  behavior is

$$W_{m,n}(s) = \sum_{k=1}^n c_k \frac{1}{s} \sum_{\ell=0}^{\infty} (-1)^\ell \left(\frac{Q_k^2}{s}\right)^\ell. \quad (\text{A5})$$

Comparing the two large  $s$  expansions, it follows that the  $c_k$  satisfy the relations



$$\sum_{k=1}^n c_k Q_k^{2\ell} = 0, \quad \ell = 0, \dots, n-m-2. \quad (\text{A6})$$

The general dispersive sum rules involving these weights, assuming  $n$  is large enough that the weighted spectral integral converges, are of course Eq. (2.9), without the factors of  $m_i$ :

$$\begin{aligned} \int_{s_{\text{th}}}^{\infty} ds W_{m,n}(s) \rho(s) &= \sum_{k=1}^n c_k \Pi(Q_k^2) \\ &= (-1)^m \sum_{k=1}^n \frac{(Q_k^2 + s_{\text{th}})^m}{\prod_{\ell \neq k} (Q_\ell^2 - Q_k^2)} \Pi(Q_k^2). \end{aligned} \quad (\text{A7})$$

The constraints of Eq. (A6) allow us to understand the cancellations involved in forming the sum that appears on the right-hand side of Eq. (A7).  $\Pi(Q^2)$  is analytic on the  $Q^2 > 0$  axis, and hence has a convergent Taylor series expansion around any point on that axis with radius of convergence the distance from that point to the start of the cut at  $Q^2 = -s_{\text{th}}$ . For illustration in what follows let us expand about the midpoint of the interval containing all pole locations,  $\tilde{Q}^2 \equiv (Q_1^2 + Q_n^2)/2$ . All of the  $Q_k^2$  then lie in the region of convergence of the Taylor expansion, and we have

$$\Pi(Q_k^2) = \sum_{\ell=0}^{\infty} \frac{1}{\ell!} \left. \frac{d^\ell \Pi(Q^2)}{d(Q^2)^\ell} \right|_{Q^2=\tilde{Q}^2} (Q_k^2 - \tilde{Q}^2)^\ell. \quad (\text{A8})$$

The (first version of the) right-hand side of Eq. (A7) then becomes

$$\sum_{\ell=0}^{\infty} \frac{1}{\ell!} \left. \frac{d^\ell \Pi(Q^2)}{d(Q^2)^\ell} \right|_{Q^2=\tilde{Q}^2} \sum_{k=1}^n c_k (Q_k^2 - \tilde{Q}^2)^\ell, \quad (\text{A9})$$

and the constraints of Eq. (A6) imply that terms in the last factor vanish for  $\ell = 0, \dots, n-m-2$ . The terms involving the derivatives of order 0 through  $n-m-2$  of  $\Pi(Q^2)$  with respect to  $Q^2$  at  $Q^2 = \tilde{Q}^2$  thus vanish, and the first surviving terms are those involving the  $(n-m-1)$ th derivative.

There is thus significant cancellation on the right-hand side of the dispersive sum rule for weights with the product-of-pole rational structure of Eq. (A1), and this cancellation gets stronger with increasing  $n-m$ . This will lead to errors on a lattice evaluation of the right-hand side which will typically increase with increasing  $n-m$ . This growth of lattice errors with increasing  $n-m$  was seen already in the dispersive analysis used to extract  $|V_{us}|$  from the experimental strange  $\tau$ -decay distribution, which employed similar product-of-pole weights, though with a constant numerator. There it was found that lattice errors could be

kept under good control for weights with 3, 4 or 5 poles, but the errors did grow as the number of pole factors increased [40].

## APPENDIX B: ISOSPIN BREAKING IN THE 3-PION CHANNEL

Experimental information on IB in the 3-pion channel is provided by *BABAR*'s vector-meson-dominance (VMD) model fit to its recent high-precision  $e^+e^- \rightarrow 3\pi$  cross sections, detailed in Ref. [64]. The VMD model for the amplitude is a sum of IC  $\omega$ ,  $\phi$ ,  $\omega'$  and  $\omega''$  resonance contributions, supplemented by an IB  $\rho$  contribution and provides an excellent fit (with  $\chi^2/\text{dof} = 136/129$ ) to the experimental cross sections in the region  $E_{\text{CM}} \leq 1.8$  GeV. The explicit model forms of the resonance contributions are as specified in Refs. [64,65]. The fit confirms the necessity of including the IB  $\rho$  contribution at the  $>6\sigma$  level. The model includes what should be the dominant (resonance-enhanced) IB contributions to the cross section in the region from threshold to slightly above the  $\phi$  resonance peak, namely the effects of  $\rho - \omega$  and  $\rho - \phi$  interference. It also includes subleading IB effects in the form of  $\rho - \omega'$  and  $\rho - \omega''$  interference contributions from the region above the  $\phi$  peak. With no IB contributions to the amplitude from the excited  $\rho$  resonances, however, it will miss IB contributions in this higher- $s$  region from, e.g.,  $\rho' - \omega'$  and  $\rho' - \omega''$  interference. Such contributions will be suppressed by the falloff with  $s$  of the weights considered in this paper and are thus also expected to be numerically subdominant.

In what follows, we take, as our estimates for the IB contributions to weighted,  $s \leq s_{\text{KNT}}$ ,  $3\pi$  spectral integrals, the results produced using the full *BABAR* VMD fit. As noted above, with the VMD model omitting terms which would model, e.g., IB  $\rho'$  and  $\rho''$  contributions to the  $3\pi$  amplitude, such estimates will miss some contributions from the region above the  $\phi$  peak. We will discuss IB in this region in more detail below and demonstrate that such missing contributions are expected to be much smaller than the uncertainties on the dominant low- $s$   $\rho - \omega$  plus  $\rho - \phi$  interference contributions, and hence that the estimates for the IB contributions to the variously weighted,  $s \leq s_{\text{KNT}}$ ,  $3\pi$  spectral integrals obtained using the *BABAR* VMD model fit are expected to be reliable within their stated errors.

The *BABAR* paper [64] contains full results for the central values and errors (though not the correlations) of the fit parameters governing the  $\omega$ ,  $\phi$  and  $\rho$  contributions to the amplitude, but not those governing the  $\omega'$  and  $\omega''$  contributions. It is thus possible to determine the  $s$  dependence of the combined  $\omega + \phi + \rho$  contribution to the VMD model representation of the cross section, but not that of the full VMD model. *BABAR* has, however, provided a table of central values of the full model representation at the midpoints of the *BABAR* experimental bins, both with the  $\rho$

contribution included and with that contribution turned off [66]. This provides us with the  $s$  dependence of the central fit values of the IB part of the VMD representation of the cross section and allows us to evaluate the central values of the variously weighted integrated versions of the IB  $3\pi$  spectral distribution of interest in this paper.

In the discussions which follow, we will denote the  $3\pi$  spectral integrals up to  $s = s_{\max}$  with the  $a_{\mu}^{\text{HVP};3\pi}$ ,  $W_{1.5}$  and  $W_{2.5}$  weights by  $a_{\mu}^{\text{HVP};3\pi}(s_{\max})$ ,  $I_{W_{1.5}}^{3\pi}(s_{\max})$  and  $I_{W_{2.5}}^{3\pi}(s_{\max})$ . The corresponding IB contributions obtained using *BABAR*'s fitted VMD model, again up to  $s = s_{\max}$ , are similarly denoted  $[a_{\mu}^{\text{HVP};3\pi}(s_{\max})]_{\text{IB}}^{\text{VMD}}$ ,  $[I_{W_{1.5}}^{3\pi}(s_{\max})]_{\text{IB}}^{\text{VMD}}$  and  $[I_{W_{2.5}}^{3\pi}(s_{\max})]_{\text{IB}}^{\text{VMD}}$ . Finally, the sums of the corresponding fully known IB VMD  $\rho - \omega$  and  $\rho - \phi$  interference contributions from the region up to just above the  $\phi$  peak (which we characterize, to be specific, as  $s \leq s_{\phi} \equiv (m_{\phi} + 4\Gamma_{\phi})^2$ ) are denoted by  $[a_{\mu}^{\text{HVP};3\pi}(s_{\phi})]_{\text{IB}}^{\rho\omega\phi;\text{VMD}}$ ,  $[I_{W_{1.5}}^{3\pi}(s_{\phi})]_{\text{IB}}^{\rho\omega\phi;\text{VMD}}$  and  $[I_{W_{2.5}}^{3\pi}(s_{\phi})]_{\text{IB}}^{\rho\omega\phi;\text{VMD}}$ , respectively.

With this notation, we find the low- $s$  IB contributions,  $[a_{\mu}^{\text{HVP};3\pi}(s_{\phi})]_{\text{IB}}^{\rho\omega\phi;\text{VMD}}$ ,  $[I_{W_{1.5}}^{3\pi}(s_{\phi})]_{\text{IB}}^{\rho\omega\phi;\text{VMD}}$  and  $[I_{W_{2.5}}^{3\pi}(s_{\phi})]_{\text{IB}}^{\rho\omega\phi;\text{VMD}}$  to represent 80%, 87% and 76%, respectively, of the corresponding full IB estimates,  $[a_{\mu}^{\text{HVP};3\pi}(s_{\text{KNT}})]_{\text{IB}}^{\text{VMD}}$ ,  $[I_{W_{1.5}}^{3\pi}(s_{\text{KNT}})]_{\text{IB}}^{\text{VMD}}$  and  $[I_{W_{2.5}}^{3\pi}(s_{\text{KNT}})]_{\text{IB}}^{\text{VMD}}$ , in line with the expectation that the IB integrals in question will be dominated by the contributions from the low- $s$  region. The full VMD-model-based IB contributions, which provide our estimates for the IB contributions to the  $s \leq s_{\text{KNT}}$ ,  $3\pi$  integrals, represent  $-1.2\%$ ,  $-1.1\%$  and  $-1.6\%$  of the corresponding  $s \leq s_{\text{KNT}}$ ,  $3\pi$  totals,  $a_{\mu}^{\text{HVP};3\pi}(s_{\text{KNT}})$ ,  $I_{W_{1.5}}^{3\pi}(s_{\text{KNT}})$  and  $I_{W_{2.5}}^{3\pi}(s_{\text{KNT}})$ , respectively.

As noted above, *BABAR* provides full information on the central values and errors only for the fit parameters determining the  $\rho$ ,  $\omega$  and  $\phi$  contributions to the  $3\pi$  amplitude, and not for those determining the  $\omega'$  and  $\omega''$  contributions. The information that is provided is, however, sufficient to allow us to study what should be the dominant uncertainties on the estimated IB  $3\pi$  contributions  $[a_{\mu}^{\text{HVP};3\pi}(s_{\text{KNT}})]_{\text{IB}}^{\text{VMD}}$ ,  $[I_{W_{1.5}}^{3\pi}(s_{\text{KNT}})]_{\text{IB}}^{\text{VMD}}$  and  $[I_{W_{2.5}}^{3\pi}(s_{\text{KNT}})]_{\text{IB}}^{\text{VMD}}$ , namely those produced by the uncertainties on the parameters entering the dominant, fully known, low- $s$  contributions,  $[a_{\mu}^{\text{HVP};3\pi}(s_{\phi})]_{\text{IB}}^{\rho\omega\phi;\text{VMD}}$ ,  $[I_{W_{1.5}}^{3\pi}(s_{\phi})]_{\text{IB}}^{\rho\omega\phi;\text{VMD}}$  and  $[I_{W_{2.5}}^{3\pi}(s_{\phi})]_{\text{IB}}^{\rho\omega\phi;\text{VMD}}$ . We find that the dominant uncertainties on these low- $s$  contributions come from the fit error in the relative phase,  $\phi_{\rho}$ , of the  $\rho$  and  $\omega$  contributions to the amplitude, which produces sizeable relative uncertainties of 87%, 92% and 70% on  $[a_{\mu}^{\text{HVP};3\pi}(s_{\phi})]_{\text{IB}}^{\rho\omega\phi;\text{VMD}}$ ,  $[I_{W_{1.5}}^{3\pi}(s_{\phi})]_{\text{IB}}^{\rho\omega\phi;\text{VMD}}$  and  $[I_{W_{2.5}}^{3\pi}(s_{\phi})]_{\text{IB}}^{\rho\omega\phi;\text{VMD}}$ . There is a smaller  $\sim 22\%$  uncertainty in all cases associated with that on the square root of  $B(\rho \rightarrow 3\pi)$ , to which the  $\rho - \omega$  and

$\rho - \phi$  interference contributions are proportional. We expect the uncertainties in the full VMD model estimates for the total IB contributions resulting from the absence of a representation of excited  $\rho$  resonance effects in the region above  $s = s_{\phi}$  to be much smaller than the dominant  $\phi_{\rho}$ -induced uncertainties, for the following reason. First, the contributions to  $a_{\mu}^{\text{HVP};3\pi}(s_{\text{KNT}})$ ,  $I_{W_{1.5}}^{3\pi}(s_{\text{KNT}})$  and  $I_{W_{2.5}}^{3\pi}(s_{\text{KNT}})$  from the region between  $s_{\phi}$  and  $s_{\text{KNT}}$  represent, respectively, only 6.6%, 3.5% and 9.4% of these totals. Even if the omitted IB  $\rho' - \omega'$ ,  $\rho' - \omega''$ , etc. interference contributions represented anomalously high 3% fractions of the total contributions from this region, they would represent only 0.20%, 0.11% and 0.28% of the corresponding  $3\pi$  spectral integral totals,  $a_{\mu}^{\text{HVP};3\pi}(s_{\text{KNT}})$ ,  $I_{W_{1.5}}^{3\pi}(s_{\text{KNT}})$  and  $I_{W_{2.5}}^{3\pi}(s_{\text{KNT}})$ , and hence only 17%, 10% and 18%, respectively, of the corresponding full VMD model IB estimates  $[a_{\mu}^{\text{HVP};3\pi}(s_{\text{KNT}})]_{\text{IB}}^{\text{VMD}}$ ,  $[I_{W_{1.5}}^{3\pi}(s_{\text{KNT}})]_{\text{IB}}^{\text{VMD}}$  and  $[I_{W_{2.5}}^{3\pi}(s_{\text{KNT}})]_{\text{IB}}^{\text{VMD}}$ , a level well below that of the dominant low- $s$ -region uncertainties. The  $s \leq s_{\phi}$ ,  $\phi_{\rho}$ -induced uncertainties thus strongly dominate the uncertainties on the estimated IB  $3\pi$  double-counting correction, especially so in the quadrature combination of the above three error contributions. Since *BABAR* does not provide the correlations between its fitted VMD parameters, and a positive  $\phi_{\rho} - B(\rho \rightarrow 3\pi)$  correlation would further increase the combined error, we assign, rather than the quadrature combination, an expanded 100% uncertainty on our integrated full VMD-model  $3\pi$  IB estimates,  $[a_{\mu}^{\text{HVP};3\pi}(s_{\text{KNT}})]_{\text{IB}}^{\text{VMD}}$ ,  $[I_{W_{1.5}}^{3\pi}(s_{\text{KNT}})]_{\text{IB}}^{\text{VMD}}$  and  $[I_{W_{2.5}}^{3\pi}(s_{\text{KNT}})]_{\text{IB}}^{\text{VMD}}$ .

From the results above, we conclude that it is possible to obtain an experimentally constrained estimate of the IB  $3\pi$  double-counting correction, albeit with an uncertainty of order 100%. This estimate is of use, despite the sizeable uncertainty, because of the small size of the central values. Explicitly, the full VMD model IB results, including this 100% uncertainty, yield

$$\begin{aligned} [a_{\mu}^{\text{HVP};3\pi}(s_{\text{KNT}})]_{\text{IB}} &= -0.54(54) \times 10^{-10}, \\ [I_{W_{1.5}}^{3\pi}(s_{\text{KNT}})]_{\text{IB}} &= -0.00041(41), \\ [I_{W_{2.5}}^{3\pi}(s_{\text{KNT}})]_{\text{IB}} &= -0.00012(12), \end{aligned} \quad (\text{B1})$$

representing  $-1.2 \pm 1.2\%$ ,  $-1.1 \pm 1.1\%$  and  $-1.6 \pm 1.6\%$ , respectively, of the full  $3\pi$  VMD contributions. As shown in the main text, the uncertainties on these corrections, even at 100%, are much smaller than the experimental uncertainties on the differences of the correspondingly weighted  $s = s_{\tau}$ ,  $2\pi + 4\pi$  electroproduction and  $\tau$  integrals. The IB  $3\pi$  double-counting correction is thus under good control for the purposes envisioned in this paper.

- [1] B. Abi *et al.* (Muon  $g - 2$  Collaboration), Measurement of the Positive Muon Anomalous Magnetic Moment to 0.46 ppm, *Phys. Rev. Lett.* **126**, 141801 (2021).
- [2] G. W. Bennett *et al.* (Muon  $g - 2$  Collaboration), Final report of the E821 muon anomalous magnetic moment measurement at BNL, *Phys. Rev. D* **73**, 072003 (2006).
- [3] T. Aoyama, N. Asmussen, M. Benayoun, J. Bijmans, T. Blum, M. Bruno, I. Caprini, C. M. Carloni Calame, M. Cè, G. Colangelo *et al.*, The anomalous magnetic moment of the muon in the Standard Model, *Phys. Rep.* **887**, 1 (2020).
- [4] T. Aoyama, M. Hayakawa, T. Kinoshita, and M. Nio, Complete Tenth-Order QED Contribution to the Muon  $g - 2$ , *Phys. Rev. Lett.* **109**, 111808 (2012).
- [5] T. Aoyama, T. Kinoshita, and M. Nio, Theory of the anomalous magnetic moment of the electron, *Atoms* **7**, 28 (2019).
- [6] A. Czarnecki, W. J. Marciano, and A. Vainshtein, Refinements in electroweak contributions to the muon anomalous magnetic moment, *Phys. Rev. D* **67**, 073006 (2003); **73**, 119901(E) (2006).
- [7] C. Gnendiger, D. Stöckinger, and H. Stöckinger-Kim, The electroweak contributions to  $(g - 2)_\mu$  after the Higgs boson mass measurement, *Phys. Rev. D* **88**, 053005 (2013).
- [8] M. Davier, A. Höcker, B. Malaescu, and Z. Q. Zhang, Reevaluation of the hadronic vacuum polarisation contributions to the Standard Model predictions of the muon  $g - 2$  and  $\alpha(m_Z^2)$  using newest hadronic cross-section data, *Eur. Phys. J. C* **77**, 827 (2017).
- [9] A. Keshavarzi, D. Nomura, and T. Teubner, Muon  $g - 2$  and  $\alpha(M_Z^2)$ : A new data-based analysis, *Phys. Rev. D* **97**, 114025 (2018).
- [10] M. Davier, A. Höcker, B. Malaescu, and Z. Zhang, A new evaluation of the hadronic vacuum polarisation contributions to the muon anomalous magnetic moment and to  $\alpha(m_Z^2)$ , *Eur. Phys. J. C* **80**, 241 (2020); **80**, 410(E) (2020).
- [11] A. Keshavarzi, D. Nomura, and T. Teubner,  $g - 2$  of charged leptons,  $\alpha(M_Z^2)$ , and the hyperfine splitting of muonium, *Phys. Rev. D* **101**, 014029 (2020).
- [12] G. Colangelo, M. Hoferichter, and P. Stoffer, Two-pion contribution to hadronic vacuum polarization, *J. High Energy Phys.* **02** (2019) 006.
- [13] M. Hoferichter, B.-L. Hoid, and B. Kubis, Three-pion contribution to hadronic vacuum polarization, *J. High Energy Phys.* **08** (2019) 137.
- [14] B.-L. Hoid, M. Hoferichter, and B. Kubis, Hadronic vacuum polarization and vector-meson resonance parameters from  $e^+e^- \rightarrow \pi^0\gamma$ , *Eur. Phys. J. C* **80**, 988 (2020).
- [15] A. Kurz, T. Liu, P. Marquard, and M. Steinhauser, Hadronic contribution to the muon anomalous magnetic moment to next-to-next-to-leading order, *Phys. Lett. B* **734**, 144 (2014).
- [16] K. Melnikov and A. Vainshtein, Hadronic light-by-light scattering contribution to the muon anomalous magnetic moment revisited, *Phys. Rev. D* **70**, 113006 (2004).
- [17] P. Masjuan and P. Sanchez-Puertas, Pseudoscalar-pole contribution to the  $(g_\mu - 2)$ : A rational approach, *Phys. Rev. D* **95**, 054026 (2017).
- [18] G. Colangelo, M. Hoferichter, M. Procura, and P. Stoffer, Rescattering Effects in the Hadronic-Light-by-Light Contribution to the Anomalous Magnetic Moment of the Muon, *Phys. Rev. Lett.* **118**, 232001 (2017).
- [19] G. Colangelo, M. Hoferichter, M. Procura, and P. Stoffer, Dispersion relation for hadronic light-by-light scattering: Two-pion contributions, *J. High Energy Phys.* **04** (2017) 161.
- [20] M. Hoferichter, B.-L. Hoid, B. Kubis, S. Leupold, and S. P. Schneider, Pion-Pole Contribution to Hadronic Light-by-Light Scattering in the Anomalous Magnetic Moment of the Muon, *Phys. Rev. Lett.* **121**, 112002 (2018).
- [21] M. Hoferichter, B.-L. Hoid, B. Kubis, S. Leupold, and S. P. Schneider, Dispersion relation for hadronic light-by-light scattering: Pion pole, *J. High Energy Phys.* **10** (2018) 141.
- [22] A. Gérardin, H. B. Meyer, and A. Nyffeler, Lattice calculation of the pion transition form factor with  $N_f = 2 + 1$  Wilson quarks, *Phys. Rev. D* **100**, 034520 (2019).
- [23] J. Bijmans, N. Hermansson-Truedsson, and A. Rodriguez-Sanchez, Short-distance constraints for the HLbL contribution to the muon anomalous magnetic moment, *Phys. Lett. B* **798**, 134994 (2019).
- [24] G. Colangelo, F. Hagelstein, M. Hoferichter, L. Laub, and P. Stoffer, Short-distance constraints on hadronic light-by-light scattering in the anomalous magnetic moment of the muon, *Phys. Rev. D* **101**, 051501 (2020).
- [25] G. Colangelo, F. Hagelstein, M. Hoferichter, L. Laub, and P. Stoffer, Longitudinal short-distance constraints for the hadronic light-by-light contribution to  $(g - 2)_\mu$  with large- $N_c$  Regge models, *J. High Energy Phys.* **03** (2020) 101.
- [26] G. Colangelo, M. Hoferichter, A. Nyffeler, M. Passera, P. Stoffer, Remarks on higher-order hadronic corrections to the muon  $g - 2$ , *Phys. Lett. B* **735**, 90 (2014).
- [27] T. Blum, N. Christ, M. Hayakawa, T. Izubuchi, L.-C. Jin, C. Jung, and C. Lehner, Hadronic Light-by-Light Scattering Contribution to the Muon Anomalous Magnetic Moment from Lattice QCD, *Phys. Rev. Lett.* **124**, 132002 (2020).
- [28] S. Borsanyi, Z. Fodor, J. N. Guenther, C. Hoelbling, S. D. Katz, L. Lellouch, T. Lippert, K. Miura, L. Parato, K. K. Szabo *et al.*, Leading hadronic contribution to the muon magnetic moment from lattice QCD, *Nature (London)* **593**, 51 (2021).
- [29] T. Blum, P. A. Boyle, V. Gülpers, T. Izubuchi, L. Jin, C. Jung, A. Jüttner, C. Lehner, A. Portelli, and J. T. Tsang (RBC and UKQCD Collaborations), Calculation of the Hadronic Vacuum Polarization Contribution to the Muon Anomalous Magnetic Moment, *Phys. Rev. Lett.* **121**, 022003 (2018).
- [30] C. Aubin, T. Blum, C. Tu, M. Golterman, C. Jung, and S. Peris, Light quark vacuum polarization at the physical point and contribution to the muon  $g - 2$ , *Phys. Rev. D* **101**, 014503 (2020).
- [31] C. Lehner and A. S. Meyer, Consistency of hadronic vacuum polarization between lattice QCD and the R-ratio, *Phys. Rev. D* **101**, 074515 (2020).
- [32] G. Wang *et al.* ( $\chi$ QCD Collaboration), Muon  $g-2$  with overlap valence fermion, [arXiv:2204.01280](https://arxiv.org/abs/2204.01280).
- [33] C. Aubin, T. Blum, M. Golterman, and S. Peris, Muon anomalous magnetic moment with staggered fermions: Is the lattice spacing small enough?, *Phys. Rev. D* **106**, 054503 (2022).
- [34] M. Cè, A. Gérardin, G. von Hippel, R. J. Hudspith, S. Kuberski, H. B. Meyer, K. Miura, D. Mohler, K. Ottnad,

- P. Srijit *et al.*, Window observable for the hadronic vacuum polarization contribution to the muon  $g-2$  from lattice QCD, *Phys. Rev. D* **106**, 114502 (2022).
- [35] C. Alexandrou, S. Bacchio, P. Dimopoulos, J. Finkenrath, R. Frezzotti, G. Gagliardi, M. Garofalo, K. Hadjiyiannakou, B. Kostrzewa, K. Jansen *et al.*, Lattice calculation of the short and intermediate time-distance hadronic vacuum polarization contributions to the muon magnetic moment using twisted-mass fermions, [arXiv:2206.15084](https://arxiv.org/abs/2206.15084).
- [36] T. Blum, P. A. Boyle, M. Bruno, D. Giusti, V. Gülpers, R. C. Hill, T. Izubuchi, Y. C. Jang, L. Jin, C. Jung *et al.*, An update of Euclidean windows of the hadronic vacuum polarization, [arXiv:2301.08696](https://arxiv.org/abs/2301.08696).
- [37] A. Bazavov, C. Davies, C. DeTar, A. X. El-Khadra, E. Gámiz, S. Gottlieb, W. I. Jay, H. Jeong, A. S. Kronfeld, S. Lahert *et al.*, Light-quark connected intermediate-window contributions to the muon  $g-2$  hadronic vacuum polarization from lattice QCD, [arXiv:2301.08274](https://arxiv.org/abs/2301.08274).
- [38] G. Colangelo, A. X. El-Khadra, M. Hoferichter, A. Keshavarzi, C. Lehner, P. Stoffer, and T. Teubner, Data-driven evaluations of Euclidean windows to scrutinize hadronic vacuum polarization, *Phys. Lett. B* **833**, 137313 (2022).
- [39] T. DeGrand, Remarks about weighted energy integrals over Minkowski spectral functions from Euclidean lattice data, *Phys. Rev. D* **106**, 014504 (2022).
- [40] P. Boyle, R. J. Hudspeth, T. Izubuchi, A. Jüttner, C. Lehner, R. Lewis, K. Maltman, H. Ohki, A. Portelli, and M. Spraggs (RBC and UKQCD Collaborations), Novel  $|V_{us}|$  Determination Using Inclusive Strange  $\tau$  Decay and Lattice Hadronic Vacuum Polarization Functions, *Phys. Rev. Lett.* **121**, 202003 (2018).
- [41] M. Hansen, A. Lupo, and N. Tantalo, Extraction of spectral densities from lattice correlators, *Phys. Rev. D* **99**, 094508 (2019).
- [42] R. Alemany, M. Davier, and A. Höcker, Improved determination of the hadronic contribution to the muon ( $g-2$ ) and to alpha  $\alpha(M_Z^2)$  using new data from hadronic  $\tau$  decays, *Eur. Phys. J. C* **2**, 123 (1998).
- [43] M. Davier, A. Höcker, G. Lopez Castro, B. Malaescu, X. H. Mo, G. Toledo Sanchez, P. Wang, C. Z. Yuan, and Z. Zhang, The discrepancy between  $\tau$  and  $e^+e^-$  spectral functions revisited and the consequences for the Muon magnetic anomaly, *Eur. Phys. J. C* **66**, 127 (2010).
- [44] F. Jegerlehner and R. Szafron,  $\rho^0 - \gamma$  mixing in the neutral channel pion form factor  $F_\pi^e$  and its role in comparing  $e^+e^-$  with  $\tau$  spectral functions, *Eur. Phys. J. C* **71**, 1632 (2011).
- [45] Z. Zhang, Review of recent calculations of the hadronic vacuum polarisation contribution, *EPJ Web Conf.* **118**, 01036 (2016).
- [46] D. Boito, M. Golterman, K. Maltman, S. Peris, M. V. Rodrigues, and W. Schaaf, Strong coupling from an improved  $\tau$  vector isovector spectral function, *Phys. Rev. D* **103**, 034028 (2021).
- [47] M. Fujikawa *et al.* (Belle Collaboration), High-statistics study of the  $\tau^- \rightarrow \pi^- \pi^0 \nu(\tau)$  decay, *Phys. Rev. D* **78**, 072006 (2008).
- [48] E. Kou *et al.* (Belle-II Collaboration), The Belle II physics book, *Prog. Theor. Exp. Phys.* **2019**, 123C01 (2019); **2020**, 029201(E) (2020).
- [49] A. Bazavov *et al.* (MILC Collaboration), Lattice QCD ensembles with four flavors of highly improved staggered quarks, *Phys. Rev. D* **87**, 054505 (2013).
- [50] N. Miller, H. Monge-Camacho, C. C. Chang, B. Hörz, E. Rinaldi, D. Howarth, E. Berkowitz, D. A. Brantley, A. S. Gambhir, C. Körber *et al.*,  $F_K/F_\pi$  from Möbius domain-wall fermions solved on gradient-flowed HISQ ensembles, *Phys. Rev. D* **102**, 034507 (2020).
- [51] B. Aubert *et al.* (BABAR Collaboration), Precise Measurement of the  $e^+e^- \rightarrow \pi^+\pi^-(\gamma)$  Cross Section with the Initial State Radiation Method at BABAR, *Phys. Rev. Lett.* **103**, 231801 (2009).
- [52] J. P. Lees *et al.* (BABAR Collaboration), Precise measurement of the  $e^+e^- \rightarrow \pi^+\pi^-(\gamma)$  cross section with the initial-state radiation method at BABAR, *Phys. Rev. D* **86**, 032013 (2012).
- [53] A. Anastasi *et al.* (KLOE-2 Collaboration), Combination of KLOE  $\sigma(e^+e^- \rightarrow \pi^+\pi^-\gamma(\gamma))$  measurements and determination of  $a_\mu^{\pi^+\pi^-}$  in the energy range  $0.10 < s < 0.95$  GeV<sup>2</sup>, *J. High Energy Phys.* **03** (2018) 173.
- [54] M. Bruno (RBC/UKQCD Collaborations), in *Proceeding of the Plenary Workshop of the g-2 Theory Initiative in Edinburgh, Scotland* (2022), <https://indico.ph.ed.ac.uk/event/112/contributions/1684/>.
- [55] S. J. Brodsky and E. De Rafael, Suggested boson-lepton pair couplings and the anomalous magnetic moment of the muon, *Phys. Rev.* **168**, 1620 (1968).
- [56] B. E. Lautrup and E. De Rafael, Calculation of the sixth-order contribution from the fourth-order vacuum polarization to the difference of the anomalous magnetic moments of Muon and electron, *Phys. Rev.* **174**, 1835 (1968).
- [57] M. Gourdin and E. De Rafael, Hadronic contributions to the muon g-factor, *Nucl. Phys.* **B10**, 667 (1969).
- [58] B. E. Lautrup, A. Peterman, and E. De Rafael, Recent developments in the comparison between theory and experiments in quantum electrodynamics, *Phys. Rep.* **3**, 193 (1972).
- [59] E. De Rafael, Hadronic contributions to the muon  $g-2$  and low-energy QCD, *Phys. Lett. B* **322**, 239 (1994).
- [60] T. Blum, Lattice Calculation of the Lowest Order Hadronic Contribution to the Muon Anomalous Magnetic Moment, *Phys. Rev. Lett.* **91**, 052001 (2003).
- [61] D. Boito, M. Golterman, K. Maltman, and S. Peris, Evaluation of the three-flavor quark-disconnected contribution to the muon anomalous magnetic moment from experimental data, *Phys. Rev. D* **105**, 093003 (2022).
- [62] J. P. Lees *et al.* (BABAR Collaboration), Measurement of the spectral function for the  $\tau^- \rightarrow K^- K_S \nu_\tau$  decay, *Phys. Rev. D* **98**, 032010 (2018).
- [63] M. Bruno, T. Izubuchi, C. Lehner, and A. Meyer, On isospin breaking in  $\tau$  decays for  $(g-2)_\mu$  from Lattice QCD, *Proc. Sci. LATTICE2018* (2018) 135.
- [64] J. P. Lees *et al.* (BABAR Collaboration), Study of the process  $e^+e^- \rightarrow \pi^+\pi^-\pi^0$  using initial state radiation with BABAR, *Phys. Rev. D* **104**, 112003 (2021).
- [65] M. N. Achasov *et al.* (SND Collaboration), Study of the process  $e^+e^- \rightarrow \pi^+\pi^-\pi^0$  in the energy region  $\sqrt{s}$  below 0.98 GeV, *Phys. Rev. D* **68**, 052006 (2003).
- [66] We thank Vladimir Druzhinin for providing this information.